FINAL TECHNICAL REPORT

U. S. Geological Survey
National Earthquake Hazards Reduction Program

Award Number 08HQGR0055

Project Title:

Characterization of Potential Seismic Sources in the Sacramento-San Joaquin Delta, California

Recipient:

Fugro William Lettis & Associates, Inc.
1777 Botelho Drive, Suite 262
Walnut Creek, California 94596

Principal Investigators:

Jeffrey R. Unruh and Christopher S. Hitchcock
Fugro William Lettis & Associates, Inc.
1777 Botelho Dr., Suite 262, Walnut Creek, CA 94596
ph: 925-256-6070;
email: unruh@lettis.com; hitch@lettis.com

Collaborators:
Scott Hector and Karen Blake
Paul Graham Drilling, Inc.
Rio Vista, CA

Term of Award:
February 1, 2008 – July 31, 2009

Research supported by the U.S. Geological Survey (USGS), Department of the Interior, under USGS award number 08HQGR0055. The views and conclusions contained in this document are those of the authors and should not be interpreted as necessarily representing the official policies, either expressed or implied, of the U.S. Government.

Abstract

The objective of this study is to evaluate subsurface, geological and topographic data to improve characterization of the Midland fault in the central Sacramento-San Joaquin Delta region as a potential seismic source. The Midland fault was active in late Cretaceous-Eocene time as a west-side-down normal fault during development of the Rio Vista basin, a structural sub-basin within the ancestral Great Valley forearc basin (Krug et al., 1992). The Midland fault has been reactivated in late Cenozoic time as a reverse fault or reverse-oblique fault in the modern transpressional tectonic setting. Existing seismic source models have assigned a range of long-term average slip rates between about 0.1 mm/yr to 1.0 mm/yr to the Midland fault, and estimated maximum magnitudes up to about **M** 6.6 (Thrust Fault Subgroup, 1999; URS, 2006). For this study, we analyzed open-hole logs from gas exploration and production wells in the central Delta region to interpret and map structural relief on the base of the Eocene-Miocene unconformity and assess late Cenozoic reactivation of the Southern Midland fault (the southern structural segment of the fault through the central Delta region as defined by URS, 2006). A structure contour map of the elevation of the basal Miocene unconformity indicates uplift of the hanging wall of the Southern Midland fault between the towns of Brentwood and Rio Vista, terminating abruptly south of Lindsey Slough in Solano County. These relations suggest a maximum potential rupture length of about 30 km for the Southern Midland fault, and associated Mmax values up to about **M** 7.2 for a range in assumptions about fault dip and maximum seismogenic depth. Structural relief on the basal Miocene unconformity across the Southern Midland fault is about 213 m (700 ft) with a maximum uncertainty of about +/- 61 m (+/-200 ft). These values suggest long-term average reverse slip rates on the Southern Midland fault ranging between about 0.07 mm/yr and 0.1 mm/yr, for an assumed range of fault dip from 45° to 75°. Comparison of structural relief on the basal Miocene unconformity with early 20th century drainage patterns reveals that the original network of small, sinuous sloughs in the Delta was primarily developed east of the Midland fault. The dendritic networks converged abruptly westward across the fault into the major channels of the San Joaquin and Sacramento Rivers. Additionally, the thickest concentrations of Holocene peat developed directly east of the Midland fault. These relations suggest that west-side-up topographic relief was present in the hanging wall of the Southern Midland fault during the late Pleistocene to Holocene time and was sufficient to affect drainage patterns and peat thickness. We interpret this as evidence for latest Pleistocene to Holocene activity on the Midland fault. From analysis of LiDAR topographic data and geotechnical borings, we infer 7 to 8 meters of structural relief on deformed late Pleistocene

deposits across the fault, suggesting a mean late Quaternary vertical separation rate between 0.2 to 0.9 mm/yr. From analysis of variations in the thickness of Holocene peat deposits from subsurface borings, we infer about 1 to 4 m of structural relief on the base of peat, suggesting a middle to late Holocene separation rate of 0.2 to 0.6 mm/yr across the southern Midland fault. Within the maximum range of uncertainty, the Holocene reverse slip rate could range up to 1.4 mm/yr, but we believe this to be highly unlikely given the very modest topographic expression of deformation in Holocene deposits and landforms, and we prefer values in the range of about 0.4 $\pm$ 0.2 mm/yr.

1.0 INTRODUCTION

This report presents the results of a neotectonic evaluation of the Midland fault in the central Sacramento-San Joaquin Delta region, California (Figure 1). This study is an outgrowth of recent work performed by the Principal Investigators for the Delta Risk Management Strategy (DRMS) Project, a comprehensive evaluation of risk from natural hazards to the Delta levee system performed by URS Corporation under the direction of the California Department of Water Resources. The results of the DRMS probabilistic seismic hazard assessment (PSHA) indicate that, as presently characterized, faults within the central Delta region pose the highest ground motion hazard to the Delta levee system (URS, 2006). The controlling sources in the central Delta region (Figure 2) at a return period of 2,500 years include:

- The Southern Midland fault;
- The Northern Midland fault zone;
- Unknown source(s) associated with the Pleistocene Montezuma Hills uplift (i.e., the "Montezuma Hills source zone")

Results of the DRMS study show that although major strike-slip faults of the San Andreas system produce larger and more frequent earthquakes than faults in the Delta, their relative contribution to hazard is lower because of their greater distance from the Delta levee system (URS, 2006).

Given the high levels of uncertainty for existing slip rate and recurrence information on faults in the Delta, conservatism in the PSHA model developed for the DRMS study cannot be reduced without collection and integration of new geologic data. The primary goal of this investigation is to acquire, analyze and synthesize new data on the Southern Midland fault and Montezuma

Hills source zone in order to: (1) improve the seismic source characterization; and (2) reduce uncertainty for refinement of the source model developed by the Northern California Working Group on Earthquake Probabilities, and the more recent PSHA developed for the Delta.

In the following sections, we summarize the geologic setting and characterization of the Midland fault and other Delta sources in the DRMS seismic source model (URS/JRB, 2008). We then present new data bearing on the style and rate of deformation associated with post-Miocene activity of the Midland fault.

NOTE: **A supplementary Appendix of correlated well logs is available for download upon request. Please contact one of the Principal Investigators for information.**

2.0 GEOLOGIC SETTING OF THE MIDLAND FAULT ZONE

The Midland fault is an approximately N- to NNW-striking, west-dipping buried or "blind" fault zone underlying the central Delta region (Figure 1). The structure is described by Krug et al. (1992) as a "complex system of branching and anatomizing normal faults" that accommodated extension and subsidence in the ancestral Great Valley forearc basin. Detailed analyses of gas well data and seismic reflection profiles document more than about 300 m (1000 ft) of west-down normal separation of Upper Cretaceous strata across the Midland fault zone (Krug et al., 1992).

The Midland fault zone is the eastern margin of a north-south-trending late Cretaceous-early Tertiary graben called the "Rio Vista basin" by Krug et al. (1992). As noted by Crane (1995), structural relationships in the subsurface of the Rio Vista basin can be inferred by examination of map-scale exposures of late Cretaceous and early Tertiary strata on the northern flank of Mt. Diablo anticline. When viewed down dip using the down-structure method (Macklin, 1950), the northeast-tilted section on the northern side of Mt. Diablo provides an approximately cross-sectional view of the upper 6-7 km of the crust (Figure 3). The exposed, tilted section flattens north of the synformal hinge at the base of the northeast limb of Mt. Diablo anticline, and has been traced beneath the central Delta region. The synformal hinge at the base of the fold thus serves as a structural "fold line", relating the cross-sectional view in the outcrop belt to the untilted section with its original upright geometry beneath the central Delta region directly to the north (Unruh et al., 2007).

As shown in Figure 3, the Kirker fault exposed in the Los Medanos Hills north of Mt Diablo is correlated with the Kirby Hills fault zone, which is the western structural margin of the Rio Vista basin. The Midland fault zone is correlated with the Brushy Creek fault mapped in the outcrop belt east of Mt. Diablo (Crane, 1995). Patterns of systematically thickening strata in the hanging walls of the main and subsidiary normal faults document syntectonic late Cretaceous and early Tertiary sedimentation. Both the Kirker and Brushy Creek faults are rooted in a low-angle fault or detachment (i.e., the Clayton fault; Figure 3) that separates relatively unmetamorphosed forearc strata above from thinned ophiolitic basement and blueschist-grade Franciscan complex below (Unruh et al., 2007). Extensional deformation in the Rio Vista basin largely ceased in Eocene time (Arleth, 1968; Krug et al., 1992), although minor normal displacement may have occurred on the Midland fault zone in late Miocene time (Weber-Band, 1998).

A small-scale generalized map by Krug et al. (1992) shows the Midland fault zone (or "system", per Krug et al., 1992) as extending for approximately 90 km (about 55 mi) from the northeastern Mt. Diablo foothills to about the latitude of the town of Dixon, CA. In detail, the Midland fault zone can be divided into southern and northern structural segments (Figures 2 and 3). The southern segment generally is south of the San Joaquin River, about 32 km (20 mi) long, strikes approximately north-south and is characterized by either a single fault trace or relatively well-defined zone of shearing (Figure 3). The northern segment strikes north-northwest and consists of a series of right-stepping en echelon traces that locally are associated with the Lindsay Slough, Maine Prairie, and Bunker gas fields. In detail, the en echelon traces are more complex than shown in the general map in Figure 3 (e.g., Division of Oil and Gas, 1982).

In addition to the major bounding faults of the graben, numerous secondary faults and splays have been identified in the Rio Vista basin during natural gas exploration and development. Two of the more significant structures include the Antioch and Sherman Island faults (Figure 3), both of which dip toward the east. Structural relations in outcrop south of the Sacramento River suggest that these two faults merge downdip and terminate downward as antithetic structures in the hanging wall of the Midland fault zone (Figure 3). Other secondary faults have been identified during exploration of the Rio Vista, Lindsay Slough and Denverton gas fields (Division of Oil and Gas, 1982; Krug et al., 1992). Many of these secondary faults strike west-northwest/east-southeast, oblique to the southern segment of the Midland fault zone; they dip toward both the northeast and southwest; and are interpreted to have been active and accommodated extension in late Cretaceous-early Tertiary time (Krug et al., 1992).

Although the Midland fault zone was thought to have been inactive in late Tertiary based on subsurface evidence for no normal faulting of Miocene and younger strata (e.g., Krug et al., 1992), subsequent work has documented evidence for post-late Miocene reactivation of the structure to accommodate reverse slip and horizontal crustal shortening. Weber-Band (1998) noted that proprietary seismic reflection profiles showed evidence of uplift and fault propagation folding of shallow reflectors above the tip of the Midland fault zone. These relationships are clearly exhibited in a seismic profile across the Midland fault zone that was published on the cover of the 1992 AAPG/SEPM guidebook entitled "Structural Geology of the Sacramento Basin" (Volume MP-41, Annual Meeting, Pacific Section, Society of Economic Paleontologists and Mineralogists, edited by V.B. Cherven and W.F. Edmondson). As this seismic line demonstrates, the folding of the shallow reflectors extends to the shallowest part of the record section, indicating very youthful folding due to reverse movement on the Midland fault zone. Normal displacement of Cretaceous and Eocene stratigraphic markers across the fault also can be observed in this seismic line, thus documenting late Cenozoic tectonic inversion of the Rio Vista basin. URS (2006) described similar relationships in other proprietary seismic lines from the central Delta region that were examined for the DRMS study. Weber-Band (1998) used a two-way time to depth conversion to estimate about 243 m of vertical separation on a late Cenozoic unconformity imaged in seismic lines due to late Cenozoic reverse slip on the Midland fault zone and uplift of the hanging wall.

The subsurface trace of the southern Midland fault lies just east of the Montezuma hills, a line of low hills bounded on the east and south by the Sacramento River (Figure 1). The Montezuma hills are capped by the Montezuma Formation, a Pleistocene fluvial deposit with a strongly developed soil, and are incised by an ephemeral drainage network. The hills are an area of anomalous positive relief in the southern Sacramento Valley and western Delta region. Weber-Band (1998) interpreted that the Montezuma hills were uplifted by late Cenozoic reverse movement on the southern Midland fault zone to the east and the Pittsburg-Kirby Hills fault zone to the west. Weber-Band (1998) identified stratigraphic marker "U1" in seismic reflection profiles across the Montezuma hills and correlated it with a 1.0 Ma tephra in the Rumsey Hills approximately 80 km (50 miles) to the north. Using the elevation of U1 in seismic time sections, Weber-Band (1998) developed a structure contour map that shows a broad, north-plunging antiformal closure bounded by the southern Midland and Pittsburg-Kirby Hills fault zones, and generally associated with the Montezuma hills. The summit elevations of interfluves in the

Montezuma hills decline gently to the north, similar to the plunge of the antiformal closure in U1 shown by Weber-Band (1998).

These interpretations of seismic reflection data are consistent with stratigraphic and structural relationships previously documented in a regional east-west cross section through the central Delta region developed by Pasquini and Milligan (1967) from open-hole logs, which shows positive relief on the unconformity at the base of the Neogene section across the Midland fault (Figure 4). Specifically, the minimum positive relief on the base of the Neogene in the cross section between the Standard Peter Cook #15 well (T.4N., R.3E., sec. 8) and the Standard Peter Cook #13 well (T.4N., R.2E., sec. 12) is about 260 m (850 ft). The total relief may be about 305 m (1000 ft) if the apparent gentle westward gradient of the base of the Neogene in the plane of the section is accounted for. This range of structural relief (260 m to 305 m) is comparable to, if somewhat higher than, the 243 m of late Cenozoic vertical separation across the fault estimated by Weber-Band (1998) from analysis of seismic reflection data.

3.0 PREVIOUS CHARACTERIZATIONS OF THE MIDLAND FAULT AS A SEISMIC SOURCE

3.1 Working Group 1999

Based on a review of available data and then-current research, the Thrust Fault Subgroup of Working Group 1999 (WG99) concluded that the Midland fault zone is a late Cenozoic active structure. Based on structural relief on late Cenozoic markers across the fault, and assumptions about the range of fault dip and onset of reverse reactivation, the Thrust Fault Subgroup (1999) developed the following range of weighted values for the late Cenozoic long-term average slip rate on the Midland fault zone:

Slip Rate (mm/yr), Midland Fault southern segment	
0.1	(0.2)
0.15	(0.6)
0.5	(0.2)

To estimate the maximum earthquake magnitude for the Midland fault zone, WG99 considered several scenarios:

1) Cumulative reverse slip during repeated earthquakes has uplifted the modern Montezuma Hills as a tectonic-geomorphic feature, according to the kinematic model of Weber-Band (1998). The maximum north-south extent of uplifted Plio-Pleistocene Montezuma Formation in the Montezuma Hills is about 20 km, implying that ruptures of comparable length may have occurred on the Midland fault;

2) Smaller segments (i.e., 10-15 km) have ruptured. If so, then it is possible that the Midland fault may have been the source of the M6 1889 Antioch area earthquake (documented in Toppozada et al., 1981);

3) The full length of the Midland fault zone mapped in the subsurface is greater than 60 km (Wagner et al., 1981; Figure 3). It is possible that a large part (i.e., about 30 km or more) of the full length of the fault ruptures in large, infrequent events.

For these scenarios, WG99 considered a weighted range of earthquake magnitudes consistent with subsurface rupture lengths corresponding to 10, 20, and 30 km (per Wells and Coppersmith, 1994):

Maximum Earthquake (Mw), Midland Fault	
6	(0.3)
$6\frac{1}{4}$	(0.4)
$6\frac{1}{2}$	(0.3)

WG99 placed the highest weight on the central value because this corresponds to an approximately 20-km-long subsurface rupture length, and is consistent with the model for uplift of the approximately 20-km-long Montezuma hills by repeated earthquakes on the Midland fault (Weber-Band, 1998).

3.2 Delta Risk Management Strategy (DRMS)

The DRMS study (URS, 2006; URS/JRB, 2008) evaluated new data and unpublished research since the Working Group 99 study and developed the following conclusions:

1) The Midland fault zone can be separated into two structural segments: (1) the Southern Midland fault, characterized by a single trace or narrow zone of shearing; and (2) a Northern Midland areal source zone (Figure 2) that encompasses the numerous right-stepping, en echelon traces mapped in the subsurface north of Rio Vista (Figure 3);
2) The north- to northeast-plunge of the folded U1 seismic marker in the Montezuma hills is not directly explained by simple reverse reactivation of the southern Midland fault, which might be expected to produce asymmetric tilting with a gradient to the west according to some models for tectonic inversion of extensional basins (e.g., McClay and Buchanan, 1992). To encompass the possibility that there may unrecognized sources other than the Southern Midland fault zone that are directly responsible for uplift and folding of the U1 marker, URS/JRB (2008) defined the "Montezuma hills areal source" zone for the regional seismic source model that included much of the Rio Vista basin the Midland fault and the Pittsburg-Kirby Hills fault zone (Figure 2).

For the DRMS study, URS (2006) evaluated unpublished California Department of Water Resources contour maps and data on elevation of the base of Holocene peat in the central Delta region. The contours show west-side-up relief on the base of peat through the central part of Franks Tract and western Webb Tract that is approximately coincident with the subsurface trace of the Midland fault zone. Regional bore-hole transect A-A' across the Delta (Figure 5; see Figure 1 for location), prepared by combining 1956 vintage CDWR borehole data from Sherman Island, Twitchell Island, Andrus Island and Venice Island, shows a possible 2-3 m west-side-up step in the contact between the base of peat/top of sand across the subsurface trace of the Midland fault zone along transect A-A'. Cross section A-A' also suggests possible east-side-up relief on the top of the sand across the Sherman Island fault.

URS (2006) also observed anomalous relief on the base of peat/top of sand above the Midland fault in a transect of borings along the southern margin of Webb Tract, directly across the San Joaquin River from transect A-A'. An updated version of the URS (2006) Webb tract transect is included in the present report as transect B-B' (Figure 6; see Figure 1 for location). Transect B-B' suggests that several meters of west-up relief may be present on the base of peat coincident with the up-dip projection of the fault tip between borings 15 and 16 (Figure 6).

The contact between the top of sand/base of peat in the boring transects (Figures 5 and 6) is a significant geologic unconformity that likely represents the Pleistocene-Holocene boundary (Atwater, 1980). The late Pleistocene landscape in the Delta formed on well-consolidated sand

during low stands of sea level. Westerly winds likely carried glacial-age flood plain or river deposits into the Delta region, forming dune fields and mantling the exposed landscape. In the Delta area, intertidal peat began to accumulate about 6,000 to 7,000 years ago (Schlemon and Begg, 1973; Drexler et al., 2006). Recent age determination of the base of the peat column in the Webb tract by Drexler et al (2006) from radiocarbon dating indicates that basal peats formed between 6,200 and 6,700 cal years BP.

Given the potential structural relief on the base of peat across the main strand of the southern Midland fault (approximately 2 m to 4 m), and the age of basal peat documented by Drexler et al. (2006), URS/JRB (2008) estimated an approximate Holocene vertical separation rate of about 0.3 to 0.6 mm/yr, given the assumption that the relief is tectonic in origin. This estimate falls within the range of 0.1-0.5 mm/yr estimated by Thrust Fault Subgroup (1999) from fold deformation of a 1.0 $\pm$ 0.5 Ma unconformity (Weber-Band, 1998), suggesting that the slip rate of the Southern Midland fault has been relatively uniform over the past million years.

URS (2006) noted that the true slip rate on the Southern Midland fault is higher if the displacement includes a component of strike separation. Recent analyses of geodetic data by Prescott et al. (2001) and d'Allessio et al. (2005) suggest that distributed NNW dextral shear associated with motion between the Pacific plate and the Sierra Nevada-Central Valley microplate may extend to the western margin of the Central Valley, and thus drive a component of strike-slip motion on the Midland fault. The DRMS study concluded that the rate of dextral-reverse oblique slip on the Midland fault may range between 0.1-1.0 mm/yr (URS/JRB, 2008).

4.0 NEW DATA AND ANALYSES

4.1 Relief on the Base of Miocene Strata in the Central Rio Vista Basin

4.1.1 Analytical Approach

As indicated by the cross section in Figure 4, positive structural relief on the basal Miocene unconformity is prima facie evidence for Neogene and/or younger uplift of the hanging wall of the southern Midland fault zone. To more fully evaluate these stratigraphic and structural relationships, we systematically analyzed open-hole electrical logs (spontaneous potential and resistivity) acquired in the central Delta region for gas exploration and development to interpret and map systematic structural relief on the base of Miocene strata across the Midland fault

zone, if any. This work was done in collaboration with Mr. Scott Hector and Ms. Karen Blake, geologists with Paul Graham Drilling, Inc., Rio Vista, CA.

Raster images of electrical logs (e-logs) for wells in the central Delta region were downloaded from an on-line database maintained by the California Division of Oil and Gas and imported into GeoGraphix, a commercial software used by the petroleum industry to analyze subsurface data. The software allows users to select arbitrary cross sections of wells, interactively define and pick stratigraphic horizons on e-logs, and save and update the picks in a database. The software can extract information from the database and generate structure contour maps of specified stratigraphic horizons.

As shown in Figure 4, the basal Miocene unconformity occurs at a depth of about 750 m to 1000 m (about 2500 ft to 3300 ft) beneath the Rio Vista basin and is characterized by subaerial fluvial deposits overlying marine deposits. Within the central Rio Vista basin, the Miocene fluvial deposits overlie the Eocene Markley Formation, a mudstone-rich marine deposit that filled a submarine gorge incised into the underlying Eocene strata (Figure 4). The Markley Formation is exposed in the east-tilted section of Cretaceous and Tertiary strata on the northeast side of Mt. Diablo anticline, south of the town of Antioch. The top of the Markley Formation consists of two map units: (1) a “siliceous shale” informally named the “Sidney Flat shale”; and (2) an overlying thin silty sand (Crane, 1988). These upper Markley units are unconformably overlain by the 11 Ma Kirker tuff and fluvial deposits of the Miocene Cierbo and Neroly Formations in the foothills of Mt. Diablo south of Antioch (Crane, 1988). The Miocene units do not appear to cut significantly downsection into the Markley Formation along structural strike in the outcrop belt.

The different textures and depositional environments of the Eocene and Miocene deposits contribute to contrasting responses on e-logs from gas wells. In general, the Markley deposits are characterized by subdued resistivity responses because the deposits are fine grained and contain relatively conductive saline brines in the pore spaces. The vertical SP profiles of the Markley strata are relatively uniform because the sediment textures do not vary significantly over short vertical distances. In contrast, the Miocene fluvial deposits are characterized by abrupt, short-wavelength vertical variations in sediment texture associated with stacked fining-upward sequences of gravels, sands and mud, and the pore spaces are filled with relatively fresh (resistive) water, all of which contributes to a much less uniform, more “chattery” appearance in the SP and resistivity logs relative to the Eocene deposits. Good examples of the contrast in e-log response between the Eocene and Miocene deposits can be seen in the

Union-W, Peter Cook-13 and Peter Cook-15 wells in Figure 4. As a first-pass interpretation of the subsurface data, we looked for this contract in the 3000 ft depth range and picked the base of the Miocene as the bottom of the “chattery” section in the e-logs.

After carefully evaluating a representative sample of e-logs from the study area, we found numerous departures from our working assumption that the base of the Miocene is consistently represented by a sharp sand/gravel-over-mudrock contact. The upper Sidney Flat shale appears to be capped by a sand in some areas (possibly a local coarsening of the upper “silty sand” unit observed in the outcrop belt to the south), thus reducing the contrast between the Markley Formation and the overlying fluvial sands and gravels on e-logs and rendering the basal Miocene contact less distinctive. Our analytical strategy was to (1) identify a cross section or suite of wells where the contact and e-log contrast is distinctive and easy to correlate from well to well; (2) establish these wells as a reference section; and (3) move laterally away from the reference section into areas where the contact is less distinctive. Where possible, we selected “loops” of wells for correlation that began and ended with the reference section. To test and improve our interpretations of the well data, we used analytical tools in GeoGraphix to flatten the correlated sections along a specified horizon and assess lateral continuity of markers directly above and below the horizon. We generally looked for continuity of at least several markers in assessing whether a given pick was correct. We also used the GeoGraphix software to generate structure contour maps of the elevation of the basal Miocene unconformity. We used these intermediate maps to identify anomalous low or high picks for review. If necessary, we reassessed our criteria for picking the basal Miocene unconformity in these regions, commonly by defining new cross-sections of wells through highs and lows in the structure contour maps and comparing picks across the anomalies. We pursued these steps iteratively to finalize our interpretation. The results are presented in a structure contour map of the basal Miocene unconformity (Figure 7) and a series of cross sections (Figures 8 and 9; see supplementary Appendix for additional cross sections shown on Figure 7, but not attached to this report).

4.1.2 Results

4.1.2.1 Extent of Post-Miocene Uplift

The structure contour map (Figure 7) indicates positive structural relief on the basal Miocene unconformity in the hanging wall of the Midland fault approximately between the towns of

Brentwood and Rio Vista, terminating abruptly southwest of Cache and Lindsey Sloughs. Positive structural relief extends about 2 km east of the subsurface trace of the Midland fault at about the latitude of the Montezuma hills. Although it is possible that these relations reflect activity on a subparallel fault trace east of the South Midland fault, we believe they are consistent with activity localized on the South Midland fault because (1) the fault trace dies out in Eocene strata below the base of the Miocene, and shallow expression of fault propagation folding in a stratigraphically higher unit would predictably be displaced updip (i.e., east) of the fault tip; and (2) the contouring program used to develop the structure map interpolates between data points, thus potentially "smearing" local relief between wells.

The uplift of the basal Miocene unconformity exhibited in the map bears a first-order similarity to the locus and geometry of uplift inferred by Weber-Band (1998) from analysis of network of crossing seismic reflection lines across the Montezuma hills. As observed by Weber-Band (1998), the uplift is broadly antiformal and plunges gently northward, terminating south of Lindsey Slough. The crest of the modern Montezuma hills similarly slopes toward the north and merges with the surrounding low topography south of Lindsey Slough. We find that the area of maximum uplift or closure is not exactly coincident with crest of the Montezuma hills, and that the culmination of the structure appears to continue south of the river beneath Bethel and Sherman Islands. If late Cenozoic surface uplift is generally coincident with positive relief on the basal Miocene unconformity, then we would expect the elevated topography of the Montezuma hills to extend south of the river. We suggest that the absence of topography is due to incision of the Sacramento and San Joaquin Rivers through uplifted late Cenozoic strata in the Bethel and Sherman Island region.

Based on the lateral extent of positive relief on the basal Miocene unconformity, we infer that the length of the Southern Midland fault that has expressed late Cenozoic reverse reactivation is about 30 km. The positive relief extends westward across the Montezuma hills. Based on previous subsurface analysis in the western Delta/Suisun Bay region by Unruh and Hector (1999), structure in the western Montezuma Hills probably is affected by uplift and tilting of the Kirby Hills along strands of the Pittsburg-Kirby Hills fault zone; thus, we infer that the influence of reverse reactivation of the Southern Midland fault extends only as far west as the central part of the Montezuma hills (Figure 7).

4.1.2.2 Post-Miocene Structural Relief

Correlated well data provide the following constraints on post-Miocene structural relief across the Southern Midland fault:

- Cross sections 1 and 2 (supplementary Appendix) trend NNW-SSE, subparallel to strike, and are located in the hanging wall and footwall of the Midland fault, respectively. Although elevation of the basal Miocene unconformity east of the Midland fault along the line of section 1 varies from -2600 ft to -3050 ft, the majority of picks cluster at a depth of about -2700 ft. The elevation of the basal Miocene unconformity also varies west of the fault in section 2 from about -1500 ft to -2700 ft, but the majority of picks occur at a depth of about -2000 ft (supplementary Appendix). Based on this visual comparison, the difference in elevation of the basal Miocene unconformity across the Midland fault is about 700 ft.
- As shown in Figure 8, cross section 4 suggests about 700 ft (+/- 200 ft) of positive relief on the basal Miocene unconformity across the Midland fault.
- As shown in Figure 9, cross section 5 suggests about 750 ft (+/- 150 ft) of positive relief on the basal Miocene unconformity across the Midland fault.
- Cross section 6 (supplementary Appendix) suggests about 650 ft (+/- 150 ft) of positive relief on the basal Miocene unconformity across the Midland fault.

Based on visual inspection of the cross sections, we conclude that a reasonable working value for the net structural relief on the basal Miocene unconformity across the Midland fault is about 700 ft, or about 213 m. This value is somewhat lower than the 243 m of late Cenozoic vertical (assumed post-Miocene) separation across the fault estimated by Weber-Band (1998) from analysis of seismic time sections. At least some of the difference can be attributed to uncertainty in estimating vertical depths from two-way time on seismic sections.

4.1.2.2 Long-Term Average Post-Miocene Slip Rate

We estimate long-term average rate of dip-slip motion on the South Midland fault from post-Miocene separation rate, and a range of assumed fault dips. For simplicity we assume that the South Midland fault is a planar structure, with the caveat that some authors infer a listric geometry for the fault (e.g., Krug et al., 1992), and that structural relief is entirely produced by dip-slip displacement. To produce total structural relief of 213 m, required reverse

displacements for fault dips of 45°, 60° and 75° are 301 m, 246 m, and 220 m, respectively. If transpressional deformation began in this region about 3 million years ago, then the long-term average reverse slip rate ranges from about 0.07 mm/yr to 0.1 mm/yr. The long-term average dip-slip rate is higher by a factor of three if the onset of transpressional deformation occurred as recently as 1.0 Ma (i.e., 0.2-0.3 mm/yr; see discussion in Weber-Band, 1998). The net slip rate also may be higher if the fault has a significant dextral component.

4.2 Relief on the Base of Holocene Peaty Deposits

Prior to historical reclamation and agricultural development, the Delta consisted of a 1,400-km^2 tidal marsh region that began forming ~6,700 years before present (Drexler et al., 2007). The top of buried Pleistocene and early Holocene deposits beneath the peat represents a subaerial landscape surface exposed prior to the rise of seawater through the Golden Gate at the beginning of the Holocene (Atwater and others, 1977; Helley and Lajoie, 1979). Basal contacts of the peat column with the underlying sediment are generally sharp (Drexler et al., 2009), and thus recognizable in well logs (e.g., Figures 5 and 6). Reconstructing the base of peat provides a datum for evaluation of potential late Quaternary fault deformation above faults, including the southern Midland fault.

4.2.1 Analytical Approach

Numerous geotechnical boreholes have been drilled 5 to 100 m deep beneath levees, within river and stream channels, and beneath farmlands in the greater Delta region. These boreholes have been completed for levee design and maintenance, residential planning, and water resource development within the central Delta region. As part of our mapping, we incorporated an in-progress database containing 1,525 borehole logs compiled by DWR Project Geology, built upon an earlier URS borehole database developed for the Delta DRMS project (pers. comm., Mark Pagenkopp, CDWR, January, 2009). We also digitized and incorporated 544 borehole and hand auger locations, including interpreted elevations of the base of peat and peaty deposits, as compiled on maps by Atwater (1982).

Out of the 1,525 borings compiled by DWR, we selected 983 borings with reliable location and elevation records that contain information on the depth to peaty deposits, the likely base of peaty deposits, or both. We combined borehole data extracted from the DWR database with locations of borehole and hand-auger borings digitized from Atwater's (1982) mapping to

construct GIS interpretative maps depicting: (1) the elevation of the top of peaty deposits; (2) elevation of the base of peaty deposits, and; (3) the inferred thickness of peaty deposits.

4.2.2 Results

4.2.2.1 Structural Relief on Holocene Peat Across Southern Midland Fault

A structure contour map on the base of peat (Figure 10) within the Delta shows a pattern of positive relief across the Southern Midland fault between the towns of Brentwood and Rio Vista. Specifically, the base of the peat is elevated in the hanging wall of the Southern Midland fault west of the updip projection of the fault tip. A similar pattern of positive relief is observed in contours on the top of peat (Figure 11). This is a younger horizon (late Holocene) than the base of peat (early to mid-Holocene), and low elevations of the horizon appear to more closely coincide with the course of the modern San Joaquin River than the older basal contact. Both the basal and upper peat stratigraphic horizons show substantial negative relief in western Webb Tract, Bouldin Island, and Venice Island, all of which are associated with the relatively downthrown footwall of the Midland fault.

The contoured net thickness of peat (Figure 12) shows that peat thins to the west across the Midland fault, coincident with the area of greatest inferred uplift, and it thickens eastward in the footwall of the fault. Peat is thickest beneath Bouldin and Venice Islands, east of Webb Tract, in the vicinity of the bend to the west of the San Joaquin River across the Midland fault (Figure 12).

We interpret these relations as evidence for Holocene activity on the Southern Midland fault. The positive relief on the base and top of peat may have been produced entirely by Holocene reverse separation on the Southern Midland fault. Alternatively, it is possible that some minor relief was present across the fault prior to onset of peat deposition to account for the west-up step in the base of peat and westward thinning of the peat. These relations imply late Pleistocene to early Holocene movement on the fault but do not necessarily support mid to late Holocene activity. However, we think the positive relief in the top of peat is best explained by mid to late Holocene (i.e., post 6.6 ka) reverse separation across the fault.

Calibrated dates of the bottom of the peat column based on radiocarbon and macrofossil age dating analyses from three localities in the direct vicinity of cross section B-B' (Figure 6) provide an age range of 6,645 to 6,720 ybp (see Figure 14 in Drexler et al., 2006). If it is assumed that

the peat has been uplifted approximately 2.4 m +/- 1.3 m across the updip projection of the fault (Figure 6), then the age of basal peat documented by Drexler et al. (2006) implies a early to mid-Holocene vertical separation rate of about 0.4 mm/yr +/- 0.2 mm/yr. This estimate of the vertical separation rate is based on offset of the base of peat deposits between borings 15 and 16 (Figure 6), with approximately 1.3 m (~4 ft) of uncertainty depending on whether the base of peat is measured solely between the two borings or inferred from the level of adjacent borings. We acknowledge that this interpretation is uncertain, however, given the highly irregular character of the basal peat/top sand contact along transect B-B'.

4.3 Geomorphic Indicators of Holocene Tectonism in the Sacramento-San Joaquin Delta

Sea level rise during the Holocene caused San Francisco Bay to fill and spread eastward through San Pablo and Suisan Bays into the Central Valley (Atwater et al., 1977). As global sea levels rose, intersection of the Sacramento and San Joaquin Rivers with tidal waters resulted in development of a subaerial network of small, sinuous tidal and non-tidal sloughs separated by extensive tidal wetlands (Atwater, 1980). This complex network of streams and sloughs drained broad areas of swampy deposits and appears to have been extremely sensitive to topography and tidal levels, providing an approximate datum for identification of local topographic anomalies and associated geomorphic features. In addition, remnants of older Eolian deposits associated with the upper member of the Modesto Formation preserved within the hanging wall of the southern Midland fault are associated with local relief and coincide with the extent of the 1850 tidal line mapped by Atwater (1982). As described in more detail below, these eolian deposits are bounded on the east by the projected tip of the Midland fault and are part of a north-trending zone of subtle topographic relief revealed in anomalous flow patterns of the Sacramento and San Joaquin Rivers across the Midland fault. We analyzed the topographic expression of these deposits to assess Holocene activity of the structure.

4.3.1 Approach

The historic and prehistoric waterways largely have been eradicated by flood control and farming, but are documented on historic 1:31,680-scale USGS topographic maps of 1908-1910 vintage (Figure 13) and partially visible on 1:6,000 to 1:24,000-scale aerial photography. The inferred traces of historic and prehistoric tidal and non-tidal waterways shown in Figure 13 were initially mapped by Atwater (1982) at 1:24,000 scale, and supplemented digitally by Hitchcock et al. (2004).

The historic topographic maps were obtained from the USGS federal center library in Denver Colorado, scanned, and georeferenced by Intec Americas Corporation. Each map was georeferenced to the Teale Albers projection. Intec digitized the 1910 topographic contours and derived a seamless digital elevation model (DEM) from these data. The original DEMs provided by Intec were recalculated by WLA staff because the algorithms used to generate the DEMs can cause incorrect topography.

The modern topographic data are derived from provisional (not final) modeled results from Light Detection and Ranging (LiDAR) flights of the Sacramento-San Joaquin Delta conducted during late January and February of 2007 under contract issued by California Department of Water Resources to URS Corporation (Joel Dudas, CDWR, January 2009, personal communciation). The aerial survey was conducted by Airborne 1 Corporation under subcontract to EarthData International, (later Fugro EarthData). Fugro EarthData completed the preliminary processing and deliverables preparation for CDWR, including the datasets obtained from CDWR via ftp in March, 2009, and subsequently incorporated for this study. The data consists of seamless, bare-earth digital elevation models (grids) with one-meter resolution and the following accuracy:

Vertical accuracy: 95% at 0.6' (<18.5 cm) and 90% at 0.5' (15 cm)

Horizontal accuracy: 1.0' (30 cm), 1 sigma.

Based on digital modern and historic topographic maps of the study area, we analyzed these topographic data along with available aerial photography in order to evaluate the distribution and expression of geomorphic landforms across the inferred surface projection of the Midland fault. For identification and analyses of the extent of peat deposits, historic tidal extent (1850 tide line, and the distribution and locations of remnant eolian deposits, we incorporated 1:24,000-scale geologic mapping by Atwater (1982), modified for our previous CALFED-funded mapping of the Delta. Atwater's (1982) mapping, originally published in map sheet format by the USGS, was digitized by the US Bureau of Reclamation for archeological research conducted between 1997 and 2001 (Hansen et al., 2001). For this study, locations of mapped eolian deposits (Atwater, 1982) with preserved, relict geomorphic expression (Hitchcock et al., 2004) were chosen for longitudinal topographic profiles.

4.3.2 Results

4.3.2.1 Comparison of Drainage Patterns with Structural Relief

Comparison of historic and pre-historic drainage patterns in the Delta with structural relief on the underlying basal Miocene unconformity provides evidence of possible Holocene uplift above the inferred tip of the southern Midland fault (e.g. Figure 13). Changes in stream flow direction and sinuosity along major and minor drainages are spatially coincident with zones of inferred uplift. Active river channels are generally coincident with apparent structural lows within the basal Miocene unconformity at depth and areas of greatest peat deposition (Figure 10). The broad east-facing monocline up-dip of the buried fault tip coincides with a historic drainage divide for minor sloughs in the Delta (Figure 13). Based on reconstruction of the drainages, sloughs in the vicinity of Holland and Franks Tracts locally flowed eastward, against the regional westward gradient but down off the local structural highs in the basal Miocene unconformity.

The dendritic network of sloughs and tributaries within the Delta fed into the major channels of the San Joaquin and Sacramento Rivers east of the fault before converging abruptly westward across the surface projection of the Midland fault (Figure 13). In addition, the relatively sinuous San Joaquin River and ancestral Old River flowed subparallel to an apparent north-trending ridge within the hanging wall of the Midland fault before merging, turning west, and crossing the fault above a structural trough in the underlying unconformity in the vicinity of Andrus Tract. Both drainages flowed northward before turning westward to cross the fault, and then southwestward towards Suisun Bay, merging with the Sacramento River. Similarly, the Sacramento River flows southward and is well constrained within natural levees upstream of the Midland fault before turning abruptly westwards to cross the fault in the vicinity of Rio Vista. This bend in the Sacramento River is coincident with underlying structural relief in the basal Miocene unconformity and, combined with the local absence of natural levee deposits which are not found across or downstream of the fault, is suggestive of local deflection of the river across a zone of active uplift in the hanging wall of the Midland fault.

Local drainage divides along the axis of the Miocene uplift and apparent deflection of flow to the north along the inferred tip of the Midland fault may reflect adjustment of the drainage system to late Pleistocene to Holocene anticlinal uplift. Based on experimental studies by Ouchi (1985), stream sinuosity typically decreases across the crest of active uplift, and increases on the upstream and downstream sides. Thus the transition from sinuous sloughs and river reaches

upstream of the Midland fault to relatively non-sinuous central stream reaches across the hanging wall of the Midland fault is consistent with Holocene uplift, coincident with convexities within the underlying basal Miocene unconformity and observed relief on the base of peaty deposits.

4.3.2.2 Late Pleistocene Eolian deposits

During the Pleistocene, westerly winds formed laterally extensive dune fields atop the exposed landscape of the ancestral Delta. The eolian sand deposits were likely derived from glacial-age flood plains of the San Joaquin and Sacramento Rivers during outwash episodes that produced the late Pleistocene Modesto Formation (Atwater, 1982), and subsequently covered by Holocene estuarine deposits of the modern Delta. The age of upper Modesto dune sand is bounded by radiocarbon dates of 40,000 and 10,000 years before present, from underlying San Joaquin River alluvium and overlying estuarine mud and peat deposits respectively, and may be as narrowly constricted as between 14,000 to 10,000 years before present if directly correlative to the alluvial fan facies of the upper member of the Modesto Formation (Atwater, 1982).

Eolian deposits of the upper member of the Modesto Formation form isolated hills in central parts of the Delta including Webb Tract (Figure 14). These hills are predominately oriented east-west, consistent with inferred wind-driven transport from the east during the Pleistocene. The eolian deposits commonly are 6 to 12 meters thick (20 to 40 feet thick) and are characterized in the subsurface by the presence of quartz-rich sand with minimal clay content. Based on available geotechnical borings and sand resource investigations within Webb Tract, eolian deposits exposed at the surface on the western portion of the island are buried by 7 to 8 meters (23-27 feet) of Holocene estuarine and fluvial deposits east of the up-dip projection of the Midland fault.

If it is assumed that the upper surface of the eolian deposits originally was a subhorizontal late Pleistocene datum, then the present relationships at Webb Tract suggest that the eolian deposits have been folded to form an east-facing monocline and subsequently overlain by the Holocene deposits east of the Southern Midland fault. The implied minimal structural relief on the top of the eolian deposits across the South Midland fault consistent with this model is about 7.5 m (25 ft), with an uncertainty of about +/- 4.6 m (+/-15 ft). These values suggest mean late Quaternary average vertical separation rates on the Southern Midland fault ranging between about 0.2 to 0.8 mm/yr, if an age range of 40,000 to 10,000 years for the eolian deposits is

utilized. The full range in separation rate, incorporating uncertainty in structural relief, is about 0.1 mm/yr to 1.2 mm/yr. The late Quaternary separation rates generally are consistent with the early to mid-Holocene rates of 0.2 to 0.6 mm/yr derived from the boring transects (Figures 5 and 6) and long-term average vertical separation rates of about 0.3 to 0.6 mm/yr estimated by URS (2006) and 0.1-0.5 mm/yr estimated by Thrust Fault Subgroup (1999), but have significantly higher uncertainties.

To further assess late Quaternary deformation of the eolian deposits, we constructed longitudinal topographic profiles along the remnant dune ridgecrests. Longitudinal profiles of axial dune remnants within tectonically stable areas typically are flat. Locally, major stratigraphic unconformities are convex or folded across the axis of uplift (e.g. Figures 5 and 7). The east-west axial profile of eolian deposits exposed on Webb Tract, south of the San Joaquin River, suggests possible broad warping within the hanging wall of the Midland fault (Y-Y'; Figure 15). Remnant ridge surfaces of the eolian dune deposits exhibit between 10 to 20 meters (about 30 to 60 feet) of net up-on-the-west relief across the up-dip projection of the Southern Midland fault. Localized relief on the eolian deposits across the Southern Midland fault coincides with a down-to-the-east step in the modified, present-day land surface of approximately two meters (6-8 feet), based on topographic profiles derived from 1-m resolution LiDAR data (Figure 15). If this relief is tectonic, then it is suggestive of Holocene displacement across the updip projection of the fault within Webb Tract.

4.3.2.3 Topographic Residual Map of Montezuma Hills

Topographic residual maps are a means of evaluating regional variations in erosional relief associated with stream incision. If it is assumed that erosional relief is a response to tectonic uplift, then residual maps indirectly document the loci and magnitude of uplift.

For this investigation, residual relief maps were derived from "envelope" and "sub-envelope" maps, using methods developed by Strahler (1952). An envelope map is an interpretation of the pre-incision landscape that is created by interpolating a smooth surface that connects interfluves and flattish summit surfaces. It is essentially a reconstruction of the pre-incision topography. In contrast, the sub-envelope map is a smooth surface formed by interpolating among the thalweg elevations of second-order drainages, and is interpreted to represent the current level of stream incision. The "residual" topography is derived by subtracting the elevation of the envelope surface from the sub-envelope surface at a point; a residual map is

the contoured values of the residuals at many points. If incision is entirely a response to tectonic uplift, then residual maps show the loci and magnitude of uplift post-dating the age of the envelope surface.

We derived envelope, sub-envelope, and residual surface maps from 10-meter USGS Digital Elevation Models (DEMs) for the Montezuma hills. Our computations were performed with the aid of ArcView 9.3 using the 3D Analyst and Spatial Analyst extensions. The reconstructed landscape, represented by the envelope map, consists of remnants of once regionally extensive erosional surfaces (Figure 16). The upper envelope surface was constructed by extracting elevations from geomorphic surfaces mapped along ridgelines in the landscape, with spot elevations derived from intersection of the surfaces with DEM data, and interpolating a gridded surface from these points. The sub-envelope surface was calculated by calculating approximate second-order stream channels from general (10-meter) DEM data, extracting spot elevations for those inferred channels, and then interpolating a gridded surface between those points. The upper envelope map confirms general field-based observations of elevated remnant geomorphic surfaces within the western, central portion of the Montezuma Hills.

The final topographic residual map (Figure 17) reveals that the maximum incision within the Montezuma hills ranges up to 54 meters within the central western portion of the hills. In addition, the observed pattern is suggestive of north- to northeastward tilting of the paleo-landscape. Although there is insufficient information to date the timing of the uplift and fluvial incision of western Montezuma hills, deep morphology of the existing canyons suggests that fluvial incision, and thus inferred structural uplift, may be ongoing.

Areas of localized high incision within the western Montezuma hills are not obviously bounded by the west-dipping Midland fault or coincident with the inferred zone of localized uplift above the Midland fault within the Delta. In addition, the pattern of stream incision across the Montezuma hills is the inverse of the inferred structural relief on the basal Miocene unconformity contoured as part of this study (Figure 7). The structure contours on the unconformity in the central western Montezuma hills form a north-northeast trending depression. This misfit between the observed surface topography versus structure at depth may be in part due to the scarcity of oil well data within the Montezuma hills, or it may reflect original pre-tectonic depositional and/or erosional relief prior to uplift.

4.3.4 Summary of Holocene Geomorphic Patterns Across the Southern Midland Fault

Interpretation of reconstructed drainage patterns, shallow geotechnical well data, and longitudinal profiles based on recent LiDAR topography provide the following constraints on loci and magnitude of late Quaternary structural relief across the Southern Midland fault:

- Deflection of streams and rivers within the Delta to the north and drainage divides separating flow within prehistoric and historic sloughs in the Delta coincide with the axis of the positive relief on the underlying Miocene unconformity, consistent with tectonic control due to Holocene reverse separation across the Midland fault.
- Relief on basal peat deposits in the central Delta region suggests a Holocene vertical separation rate of about 0.2 to 0.6 mm/yr.
- Inferred structural relief on the top of the eolian deposits across the Southern Midland fault is about 8 m (25 ft), suggest mean late Quaternary vertical separation rates between about 0.2 to 0.8 mm/yr, with a full range of 0.1-1.2 mm/yr incorporating all uncertainty.

5.0 Conclusions: Updated Source Characterization for the Southern Midland Fault

New work presented in this report provides a basis for updating the recent URS/JRB (2008) characterization of the Southern Midland fault as a seismic source for the DRMS study.

Subsurface mapping for this study confirms previous work summarized in WG99 and URS (2006) that the Southern Midland fault has been reactivated in late Cenozoic time as a reverse or reverse-oblique fault. New analysis herein documents evidence for mid- to late Holocene activity.

The maximum rupture length of the Southern Midland fault appears to be limited to about 30 km, based on the extent of post-Miocene uplift of the hanging wall of the fault. Empirical relations among earthquake magnitude and rupture length for reverse faults in Wells and Coppersmith (1994) suggest an associated maximum magnitude of **M** 6.8. If it is assumed that the seismogenic crust is about 20 km thick in this region, and that the fault dips 70° to the west, then the maximum potential rupture area for a 30-km-long rupture is about 1754 km^2. The empirical relation between rupture area and magnitude for reverse faults in Wells and Coppersmith (1994) indicates a maximum earthquake of **M** 7.24. Both of these estimates are

higher than the weighted mean magnitude of **M** 6.6 adopted by URS/JRB (2008) for the Southern Midland fault.

Although slip rate for the Southern Midland fault is determined indirectly and is highly uncertain, most estimates for reverse slip rate based on fold deformation of early Quaternary (about 1.0 Ma) and Holocene (post 6.6 ka) stratigraphic datum fall in a range of about 0.3 $\pm$ 0.2 mm/yr. Within the maximum range of uncertainty, the Holocene reverse slip rate could range up to 1.4 mm/yr, but we believe this to be highly unlikely given the very modest topographic expression of deformation in Holocene deposits and landforms, and we prefer values in the range of about 0.4 $\pm$ 0.2 mm/yr.

The true slip rate on the Southern Midland fault could potentially be several times higher than 0.4 $\pm$ 0.2 mm/yr if there is a significant component of right-lateral motion on the fault. This possibility was incorporated in the DRMS model and represented by a 0.3 weighting assigned to a reverse-oblique slip rate of 1.0 mm/yr (URS/JRB, 2008). Although this study did not develop data to directly address sense of slip on the Southern Midland fault, we note that there is no increased uplift at the northern end of the structure where it takes a slight bend to the west. This change in strike is a restraining geometry in a right-lateral regime, and all things being equal may be expected to generate localized shortening and increased uplift of the northwestern Montezuma Hills relative to areas to the south. The fact that the opposite trend is observed suggests that the dextral component on the fault is small or non-existent, and/or that the uplift of the Montezuma hills is controlled by other cryptic structures in addition to the Southern Midland fault.

6.0 Acknowledgements

Support for this research was provided to Fugro William Lettis & Associates, Inc., by a grant from the Department of Interior, U.S. Geological Survey (National Earthquake Hazards Reduction Program, contract award 08HQGR0055). The contents of this report do not necessarily represent the policy of the U.S. Geological Survey, however, and the endorsement of the federal government should not be assumed. We appreciate data provided by CDWR, including support from Mark Pagenkopp and Frank Glick of CDWR's Project Geology Branch.

7.0 References Cited

Arleth, K.H., 1968, Maine Prairie gas field, Solano County, California, in Beebe, B. W., and Curtis, B.F., eds. Natural Gases of North America: American Association of Petroleum Geologists Memoir 9, vol. 1, p. 79-84.

Atwater, B.F., Hedel, C.W., Helley, E.J., 1977, Later Quaternary depositional history, Holocene sea-level changes, and vertical crustal movement, Southern San Francisco Bay, California: US Geological Survey Professional Paper 1014, 15 p.

Atwater, B. F., 1980, Attempts to correlate Late Quaternary climatic records between San Francisco Bay, the Sacramento-San Joaquin Delta, and the Mokelumne River California, University of Delaware, Ph.D dissertation, 215 p.

Atwater, B.F., 1982, Geologic maps of the Sacramento-San Joaquin Delta, California: U.S. Geological Survey Miscellaneous Field Studies Map - U.S. Geological Survey: MF-1401, 21 sheets.

Crane, R., 1988, Geologic map of the Antioch South 7.5-minute quadrangle: unpublished map available from H&L Hendry, Concord, CA; scale 1:24,000.

Crane, R.C., 1995, Geology of the Mt. Diablo region and East Bay hills, in Sangines, E.M., Andersen, D.W., and Buising, A.V., eds., Recent Geologic Studies in the San Francisco Bay Area: Society of Economic Paleontologists and Mineralogists, Pacific Section Volume 76, p. 87-114.

d'Alessio, M. A., Johanson, I. A., Bürgmann, R, Schmidt, D. A., and M. H. Murray. 2005, Slicing up the San Francisco Bay Area: Block kinematics and fault slip rates from GPS-derived surface velocities. Journal of Geophysical Research 110, doi:10.1029/2004JB003496.

Drexler, J Z, Verosub, K L, Delusina, I, de Fontaine, C S, Lunning, N, Wong, S, 2006, Project REPEAT: Rates and Evolution of Peat Accretion through Time in the Sacramento- San Joaquin Delta, California: Eos Trans. AGU, 87(52), Fall Meet. Suppl., Abstract PP 51A-1125.

Drexler, J.Z., C.S. de Fontaine, and D.L. Knifong, 2007, Age determination of the remaining peat in the Sacramento–San Joaquin Delta, California, USA. US Geological Survey Open File Report 2007-1303, Sacramento, California.

Drexler, J.Z., C.S. de Fontaine, and T.A. Brown, 2009, Peat Accretion Histories During the Past 6,000 Years in Marshes of the Sacramento–San Joaquin Delta, CA, USA: Estuaries and Coasts, v. 32, pp. 871–892.

Division of Oil and Gas, 1982, Oil and Gas Fields, Northern California: Volume 3 of Publication TR10, State of California, Sacramento.

Hansen, D.T., West, J., Welch, P, and B. Simpson, 2001, Geomorphology_Delta.mdb - Geology of the Sacramento - San Joaquin Delta, California: U.S. Bureau of Reclamation, Mid-Pacific Region, MPGIS Service Center, digital database available via: http://gis.ca.gov/catalog/BrowseRecord.epl?id=29584

Helley, E.J., and Lajoie, K.R., 1979, Flatland deposits of the San Francisco Bay Region, California - Their geology and engineering properties, and their importance to comprehensive planning: United States Geological Survey Professional Paper 943.

Hitchcock, C.S., Helley, E., and Givler, R., 2004, Geomorphic and geologic mapping for restoration planning, Sacramento-San Joaquin Delta Region: Proceedings of the 2004 CALFED Bay-Delta Program Science Conference.

Krug, E.H., Cherven, V.B., Hatten, C.W., and Roth, J.C., 1992, Subsurface structure in the Montezuma Hills, southwestern Sacramento basin, in Cherven, V.B., and Edmondson, W.F., eds., Structural Geology of the Sacramento Basin: Volume MP-41, Annual Meeting, Pacific Section, Society of Economic Paleontologists and Mineralogists, p. 41-60.

Macklin, J.H., 1950, The down-structure method of viewing geologic maps: Journal of Geology, v. 58, p. 55-72.

McClay, K.R., and Buchanan, P.G., 1992, Thrust faults in inverted extensional basins, in McClay, K.R., ed., Thrust Tectonics: Chapman and Hall, London, England, p. 93-104.

Pasquini, D.E., and Milligan, H.L., 1967, Correlation Section 15, Sacramento Valley, Suisun Bay to Lodi: Pacific Section, American Association of Petroleum Geologists.

Prescott, W.H., Savage, J.C., Svarc, J.L., and Manaker, D., 2001, Deformation across the Pacific-North American plate boundary near San Francisco, California: Journal of Geophysical Research, v. 106, no. B4, p. 6673-6682.

Shlemon, R. J., and E. L. Begg. 1973, Late Quaternary evolution of the Sacramento-San Joaquin Delta, California: Proc. Ninth Congress of the International Union for Quaternary Research 1973:259-266.

Strahler, A.N., 1952, Dynamic basis of geomorphology: Geological Society of America Bulletin, v. 63, p. 923-938.

Thrust Fault Subgroup 1999, Report to the Working Group on Northern California Earthquake Probabilities, 15 p. plus tables.

Toppozada, T. R., Real, C. R., and Parke, D. L., 1981, Preparation of isoseismal maps and summaries of reported effects for pre-1900 California earthquakes: California Division of Mines and Geology Open-File Report 81-11 SAC, p. 107-109, 164.

Unruh, J.R., and Hector, S.T., 1999, Subsurface Characterization of the Potrero-Ryer Island Thrust System, Western Sacramento-San Joaquin Delta, Northern California: Final Technical Report submitted to the U.S. Geological Survey, National Earthquake Hazards Reduction Program award number 1434-HQ-96-GR-02724, 32 p.

Unruh, J. R., Dumitru, T. A., and Sawyer, T. L., 2007, Coupling of early Tertiary extension in the Great Valley forearc basin with blueschist exhumation in the underlying Franciscan accretionary wedge at Mount Diablo, California**:** Geological Society of America Bulletin, v. 119, no. 11/12, p. 1347 - 1367.

URS Corporation, 2006, Technical Memo, Probabilistic Seismic Hazard Analysis: report submitted to the California Department of Water Resources, 40p.

URS Corporation/Jack R. Benjamin and Associates, Inc., 2008, Delta Risk Management Strategy, Phase 1, Risk Analysis Report: Prepared for the California Department of Water

Resources, available on-line at this URL: http://www.water.ca.gov/floodmgmt/dsmo/sab/drmsp/phase1_information.cfm

Wagner, D.L., Jennings, C.W., Bedrossian, T.L., and Bortugno, E.J., 1981, Geologic map of the Sacramento Quadrangle: California Division of Mines and Geology Regional Geologic Map Series, 1:250,000 scale.

Wagner, D.L., Bortugno, E.J., and McJunkin, R.D., 1991, Geologic map of the San Francisco-San Jose quadrangle: California Division of Mines and Geology, Regional Geologic Map Series, 1:250,000 scale.

Weber-Band, J., 1998, Neotectonics of the Sacramento-San Joaquin Delta area, east-central Coast Ranges, California: Ph.D. dissertation, University of California, Berkeley, 216 p.

Wells, D. L., and Coppersmith, K. J., 1994, New empirical relationships among magnitude, rupture length, rupture width, rupture area, and surface displacement: Seismological Society of America Bulletin, v. 84, no. 4, p. 974-1002.

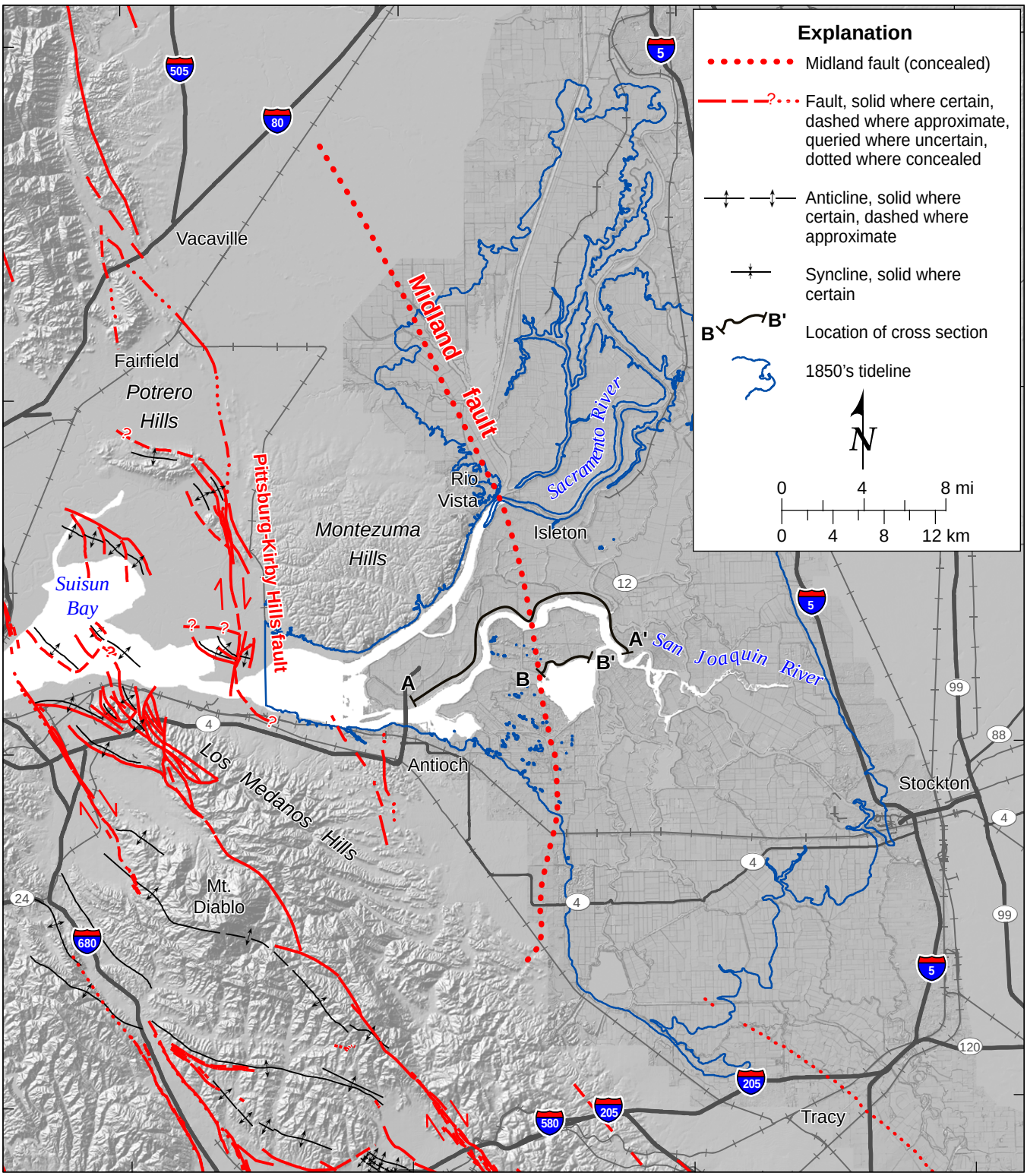

Graphics, Active Projects, 1958.000 Midland Fault, Modified 10.26.09

Location Map

FIGURE 1

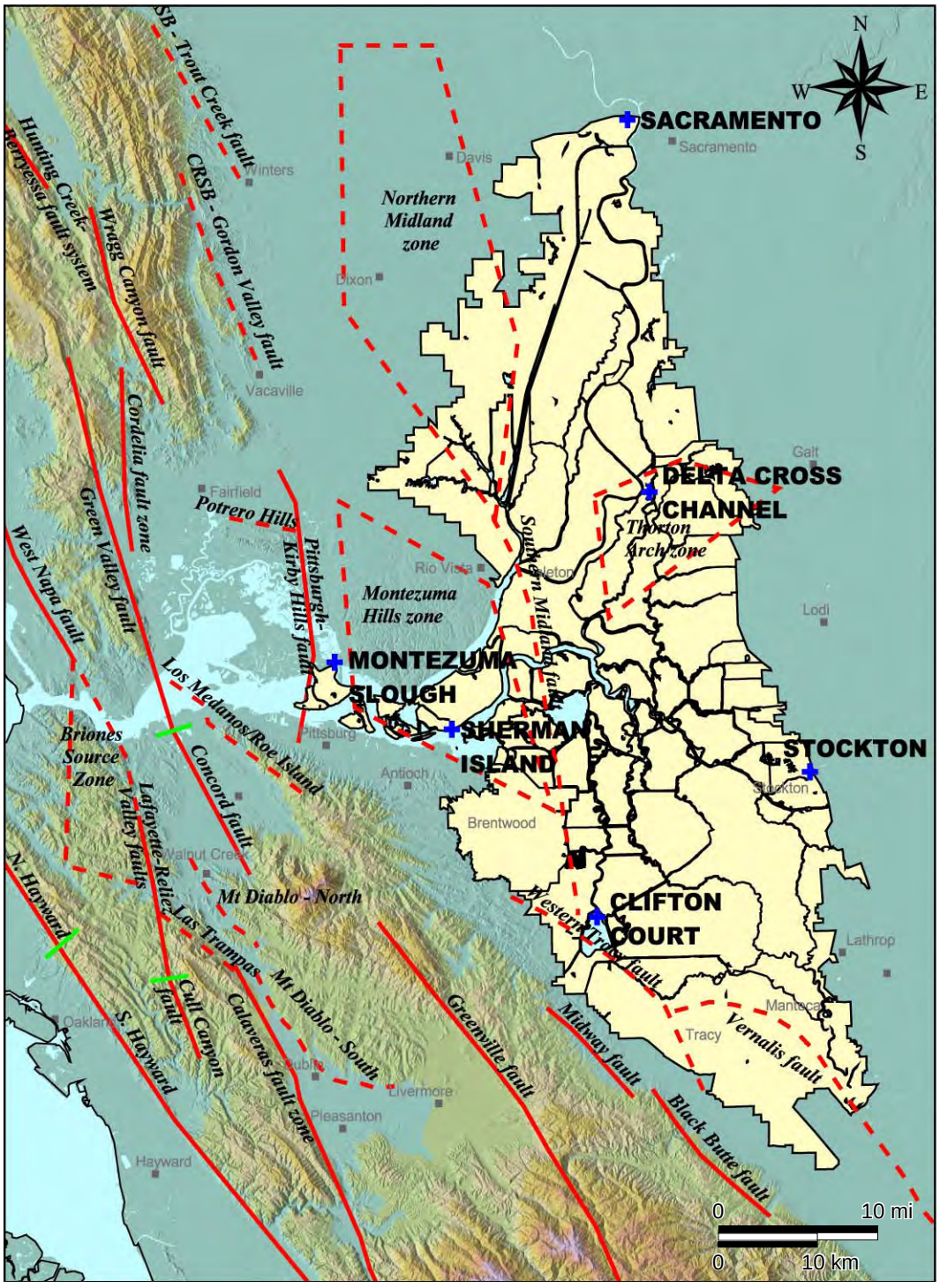

Explanation

- Legal Delta Boundary V. 2002-4
- Surficial fault used in the hazard analysis
- Blind fault used in the hazard analysis
- Bounds of delta islands
- *CRSB* — Coast Range Sierran Block

Note: Major seismic sources and source zones in the greater Delta region included in the seismic hazard model for the Delta Risk Management Study project (figure modified from URS, 2007).

Seismic Sources in the Greater Delta Region FIGURE 2

Graphics, Active Projects, 1958.000 Midland Fault, Modified 10.14.09

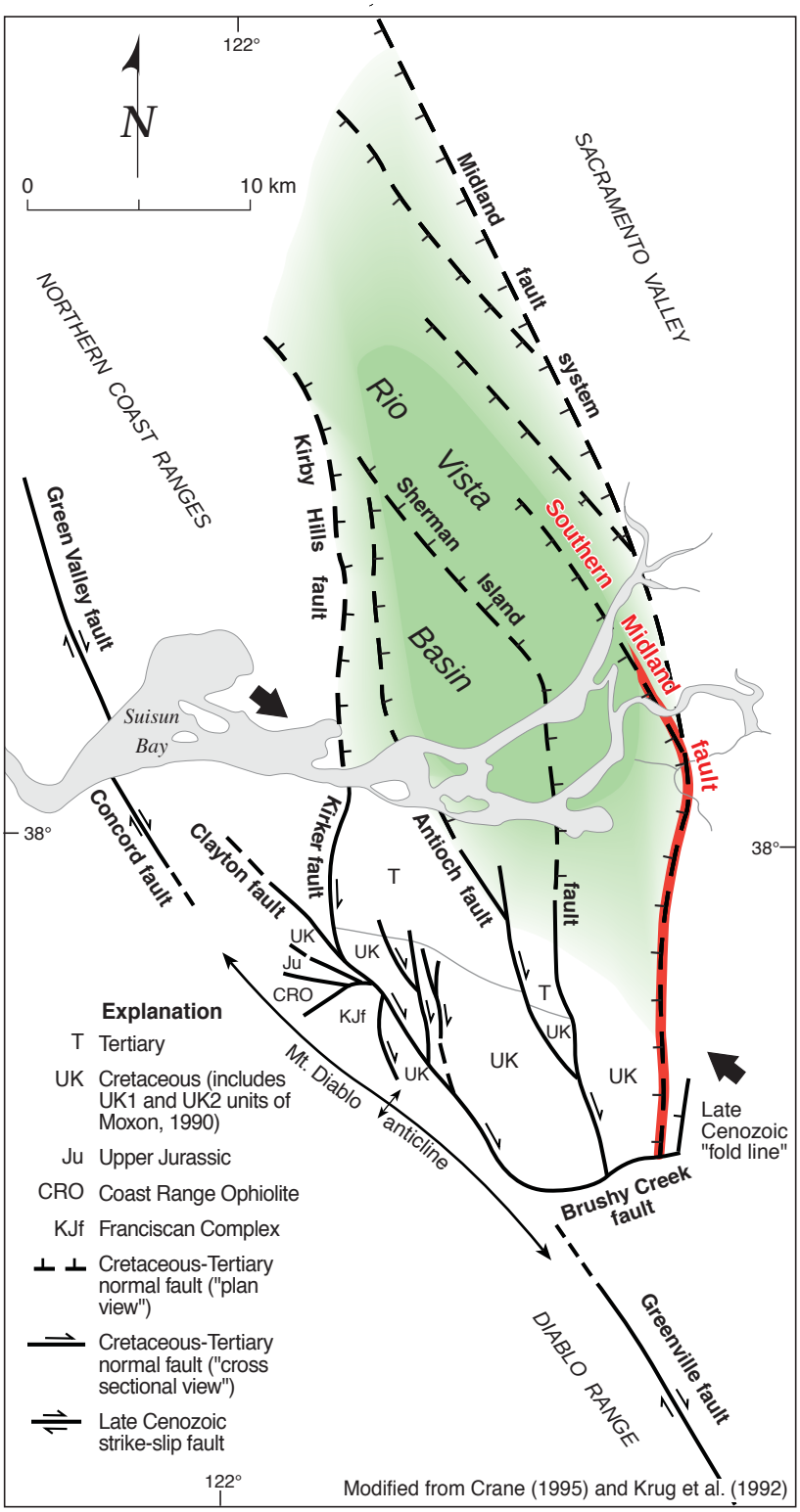

Note: Figure modified from Unruh et al., (2007) showing the location of the Rio Vista basin, the Midland fault zone, and the relationship of structures in the subsurface of the Delta to faults exposed on the northeastern flank of Mt. Diablo anticline.

Graphics, Active Projects, 1958.000 Midland Fault, Modified 10.14.09

Geologic Structure of the Rio Vista Basin FIGURE 3

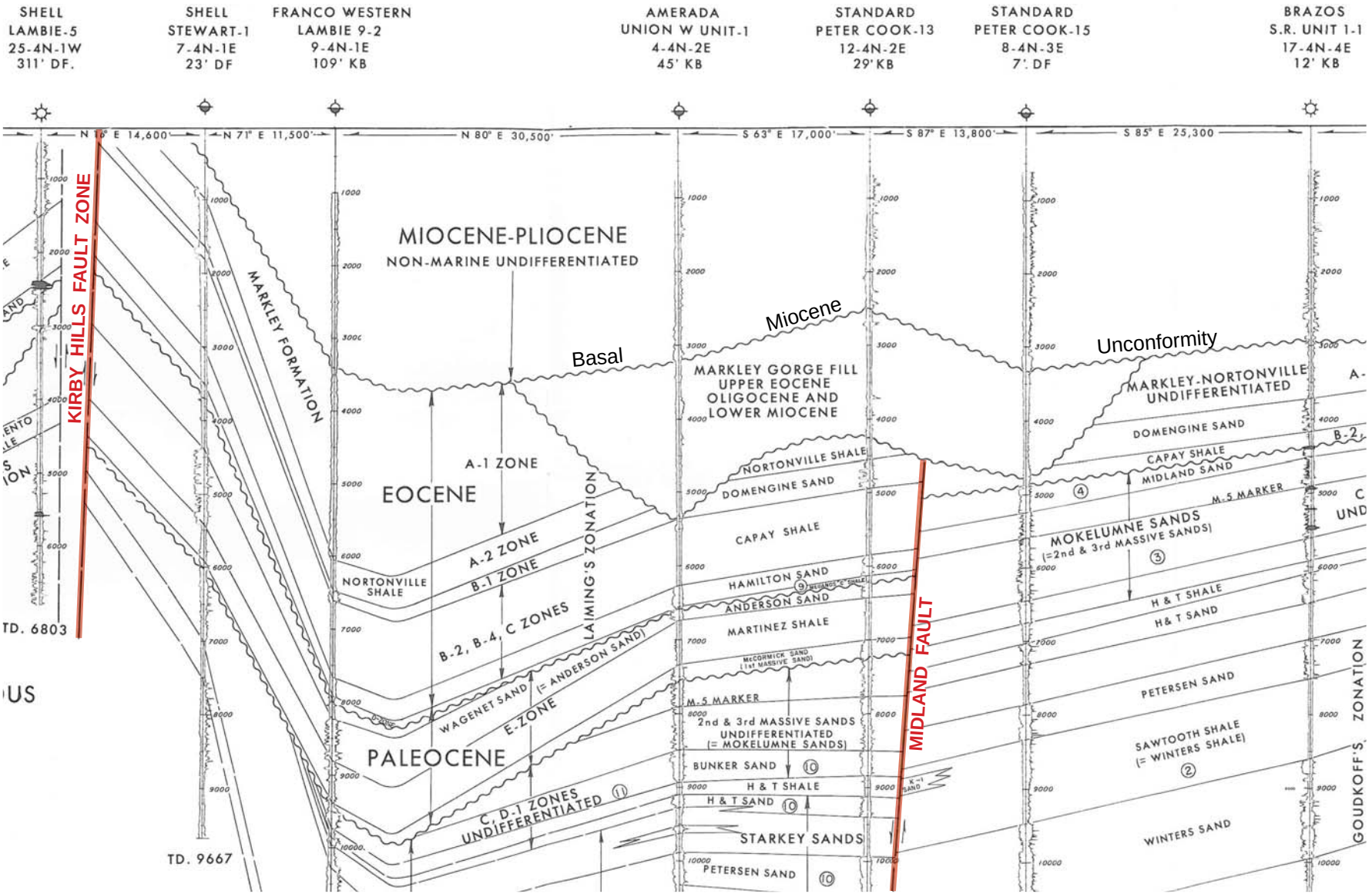

Note the positive structural relief on the basal Miocene unconformity across the Midland fault consistent with late Cenozoic reverse motion, in contrast to the normal separation of Eocene and older units.

Part of a Regional East-west Cross Section through the Central Delta Region Developed by Pasquini and Milligan (1967) from Analysis of Open-hole Logs

FIGURE 4

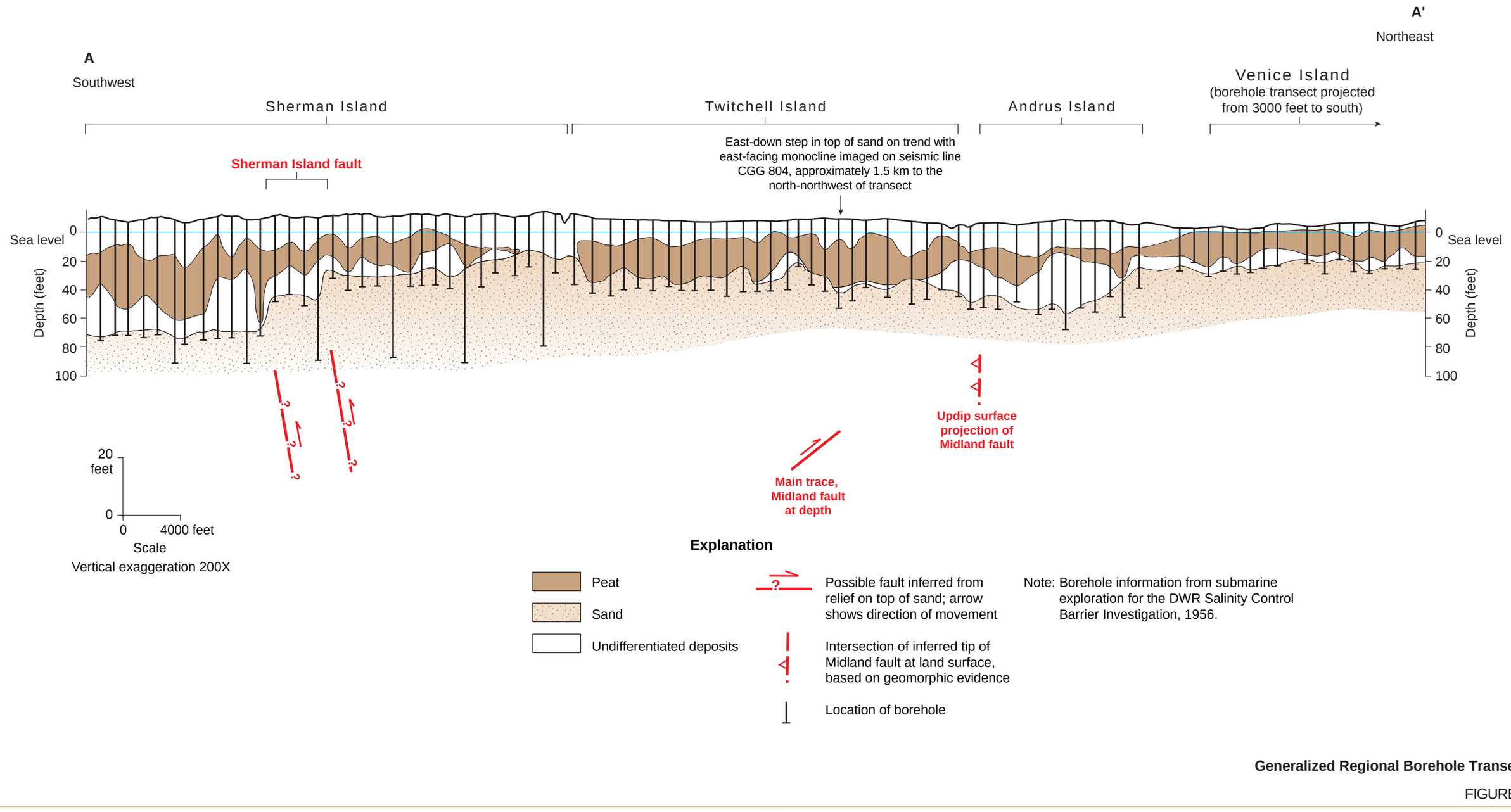

Graphics, Active Projects, 1958.000 Midland Fault, Modified 10.16.09

Generalized Regional Borehole Transect

FIGURE 5

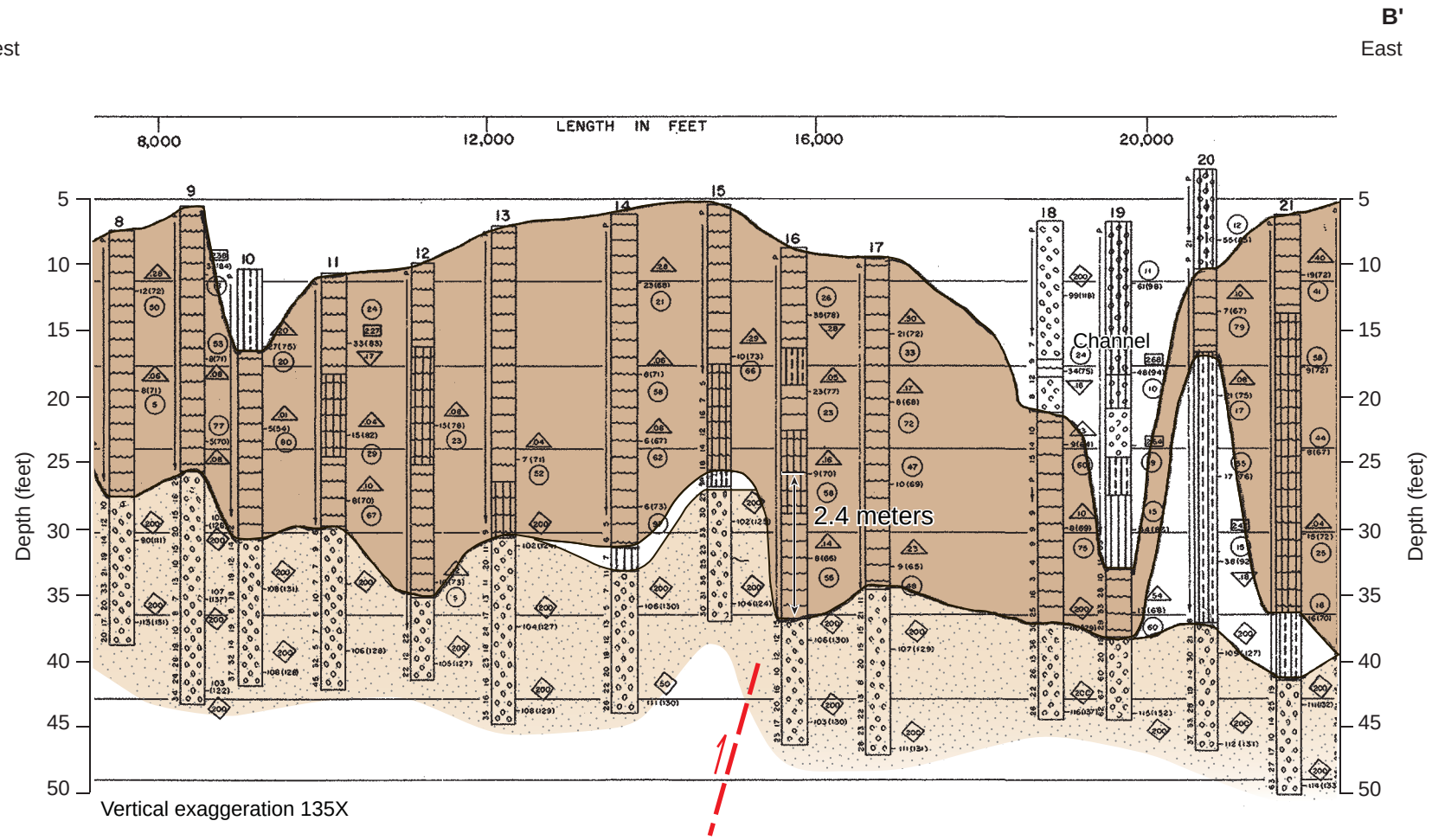

Explanation

- Peat
- Sand
- Undifferentiated deposits
- Subsurface trace of the Midland fault (this study)

Note: Base scan from DWR Salinity Control Barrier Investigation, Primary Subsurface Exploration on Webb Tract (drilling dates December 30, 1957 to June 19, 1958).

Geologic Transect along Webb Tract across the Midland Fault

FIGURE 6

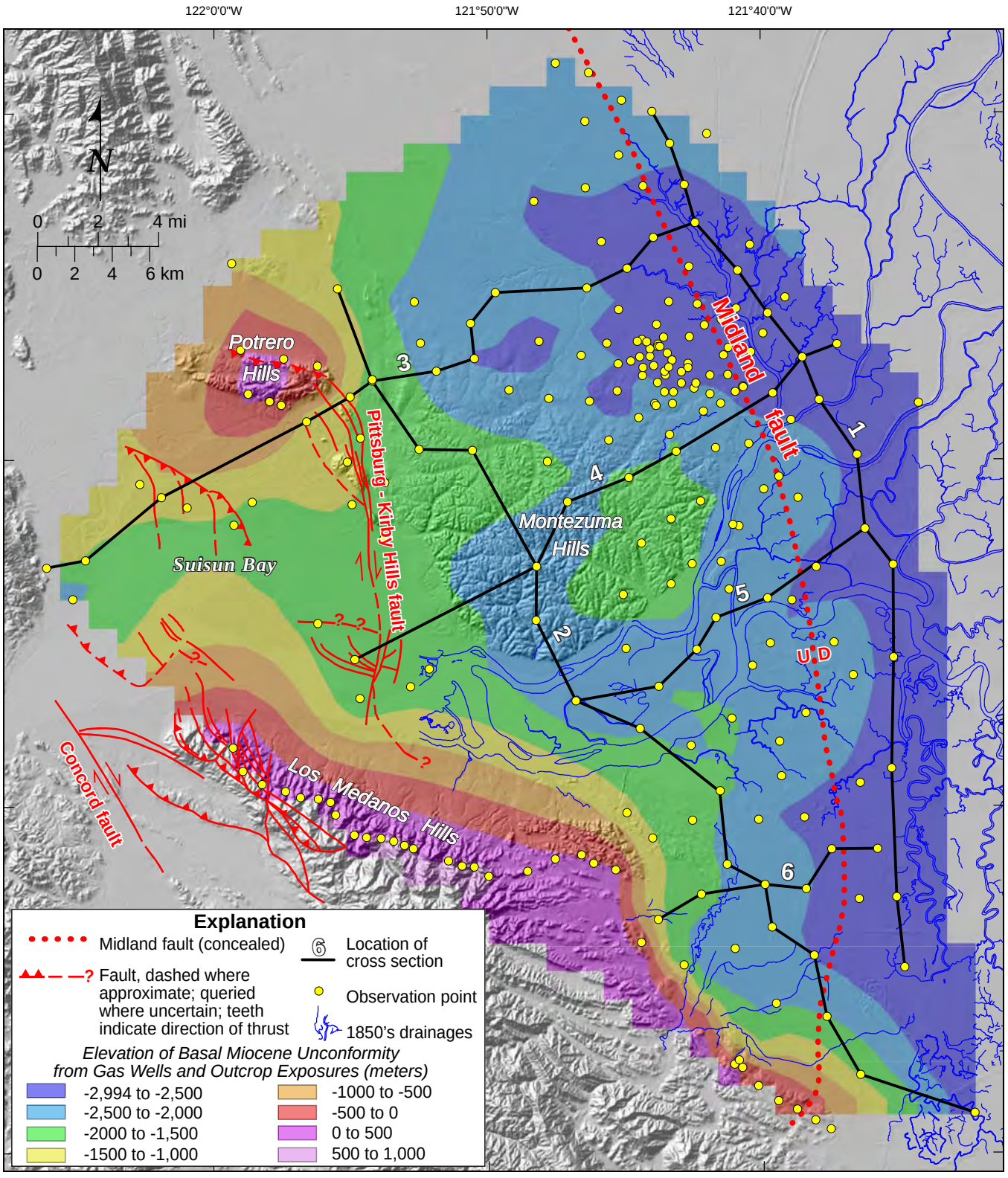

Graphics, Active Projects, 1958.000 Midland Fault, Modified 10.14.09

Structure Contour Map of Basal Miocene Unconformity FIGURE 7

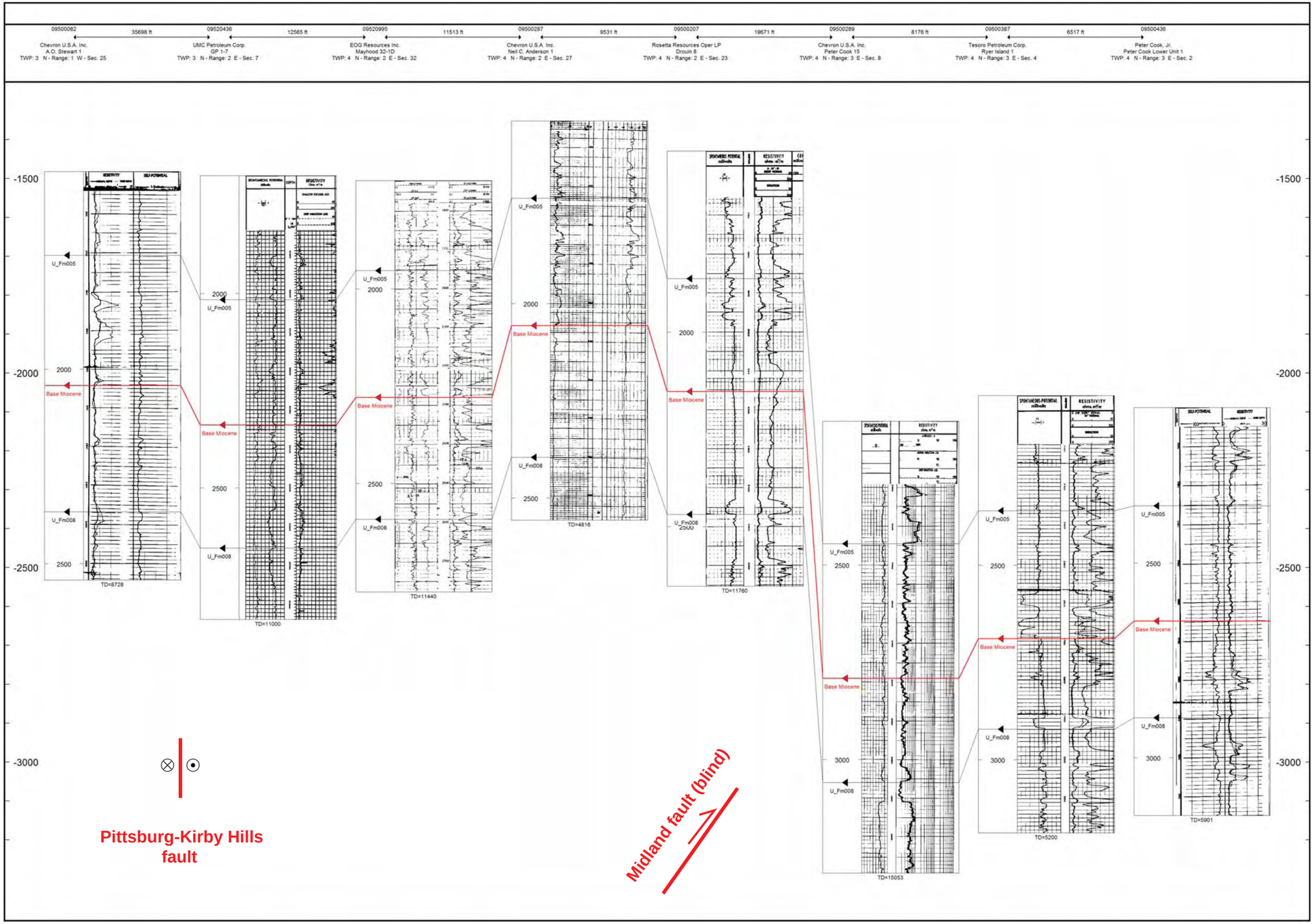

Note: See Figure 7 for location of cross section.

**Cross Section 4
with Interpreted Structural Relief
on the Basal Miocene Unconformity**

FIGURE 8

Graphics, Active Projects, 1958.000 Midland Fault, Modified 10.14.09

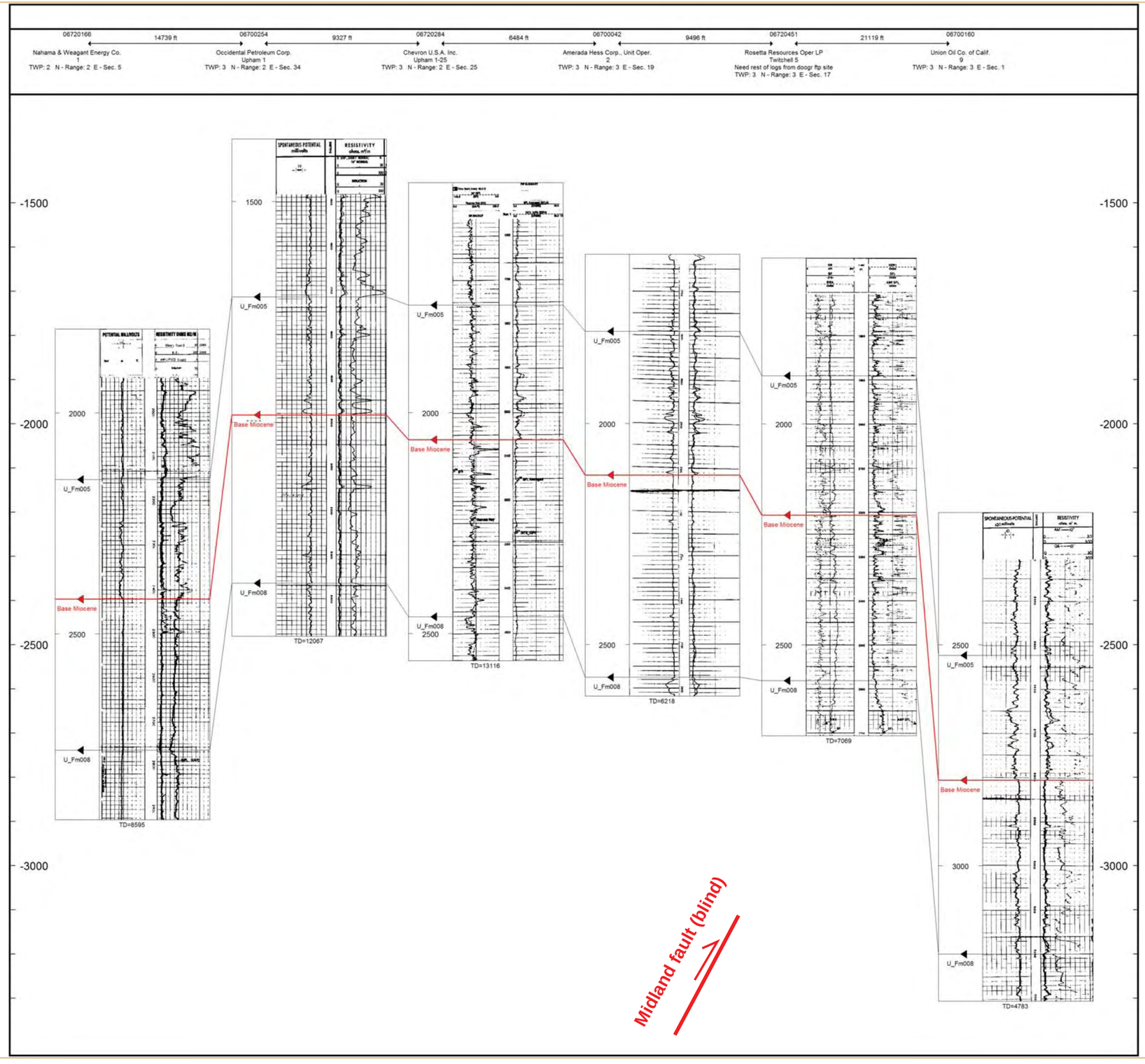

Note: See Figure 7 for location of cross section.

Cross Section 5
with Interpreted Structural Relief
on the Basal Miocene Unconformity

FIGURE 9

Graphics, Active Projects, 1958.000 Midland Fault, Modified 10.14.09

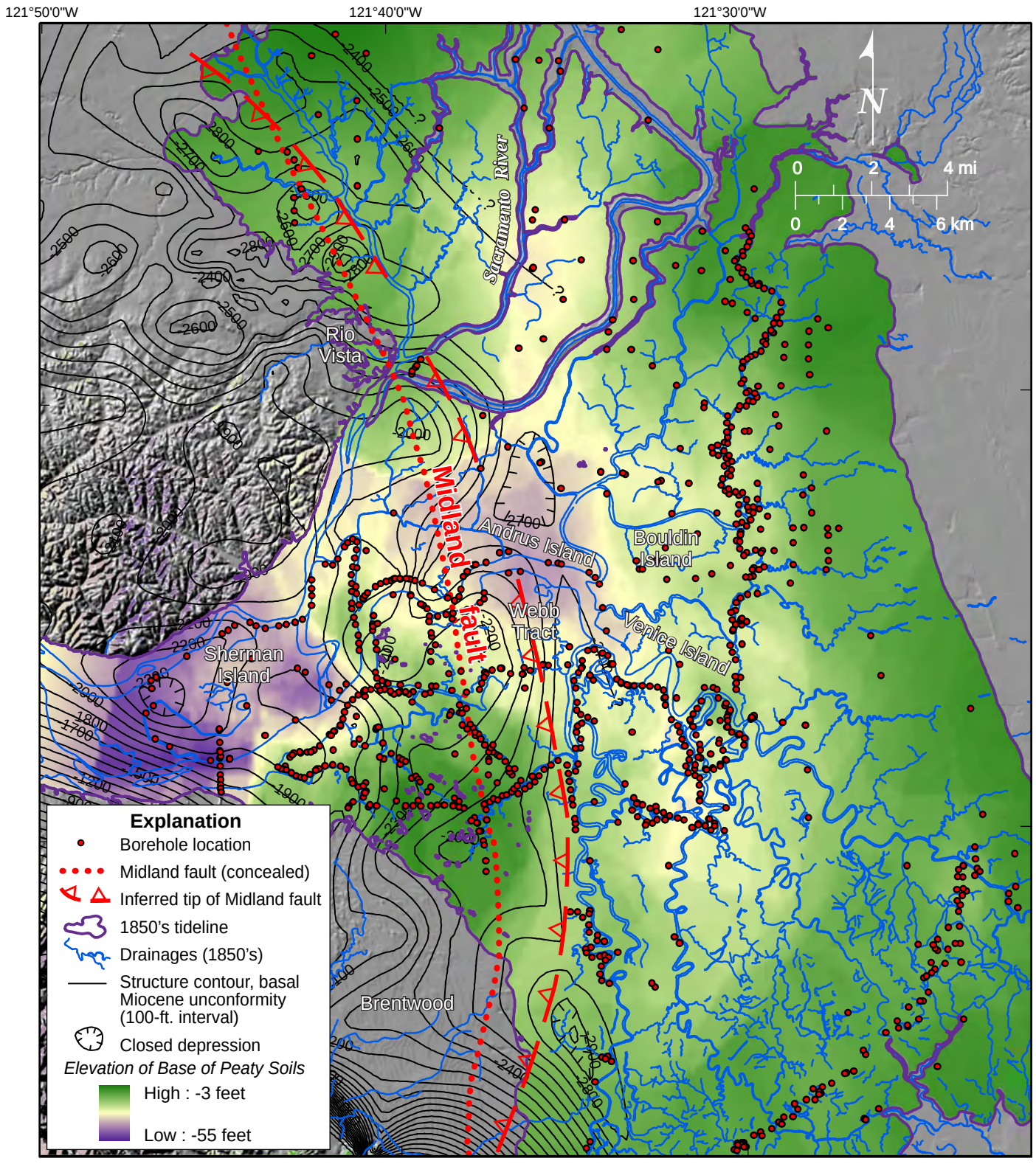

Graphics, Active Projects, 1958.000 Midland Fault, Modified 11.15.09

Structure Contours Shown on Base of Peaty Soils FIGURE 10

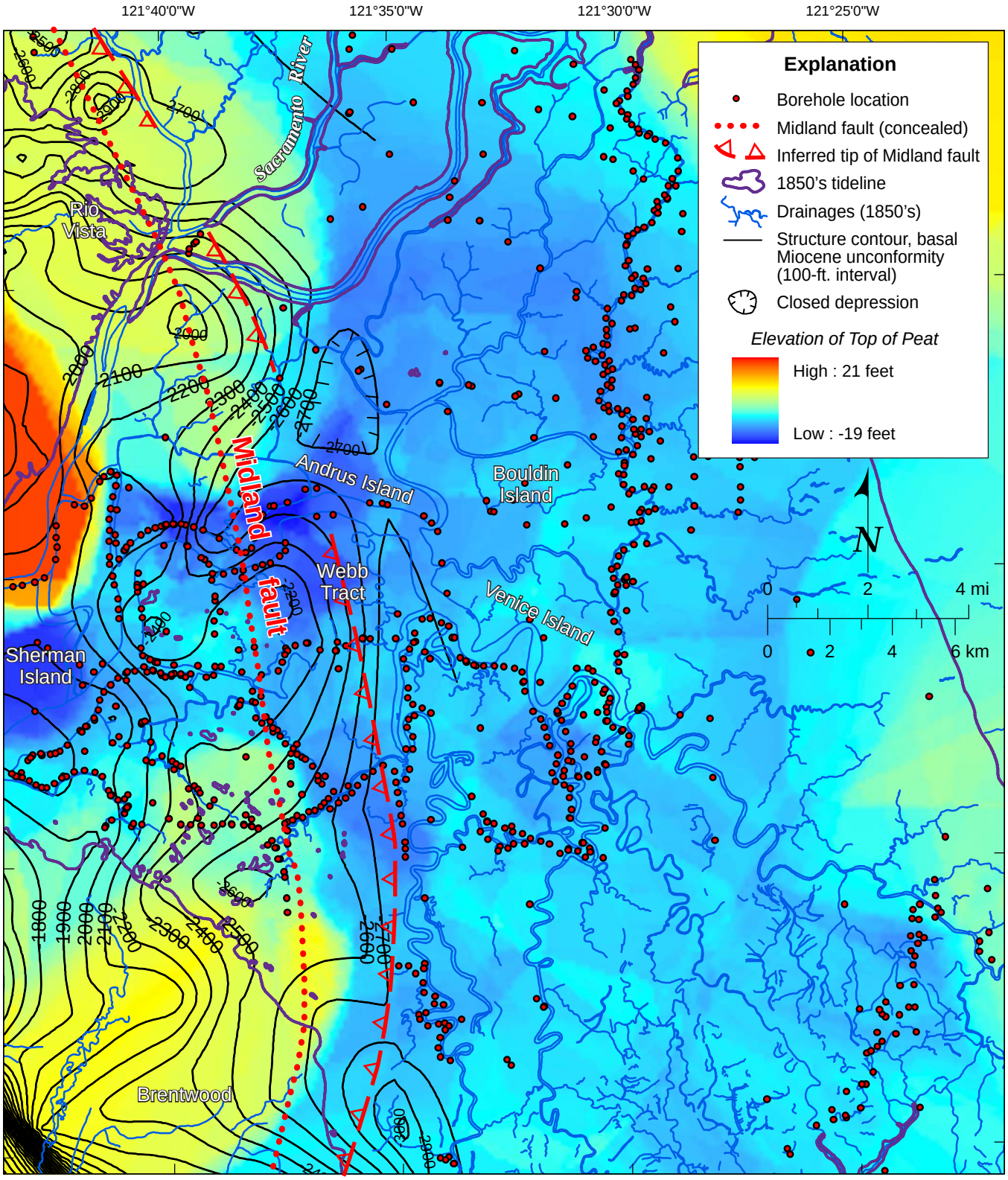

Graphics, Active Projects, 1958.000 Midland Fault, Modified 11.15.09

Elevation of Top of Peat versus Relief on Basal Miocene Unconformity FIGURE 11

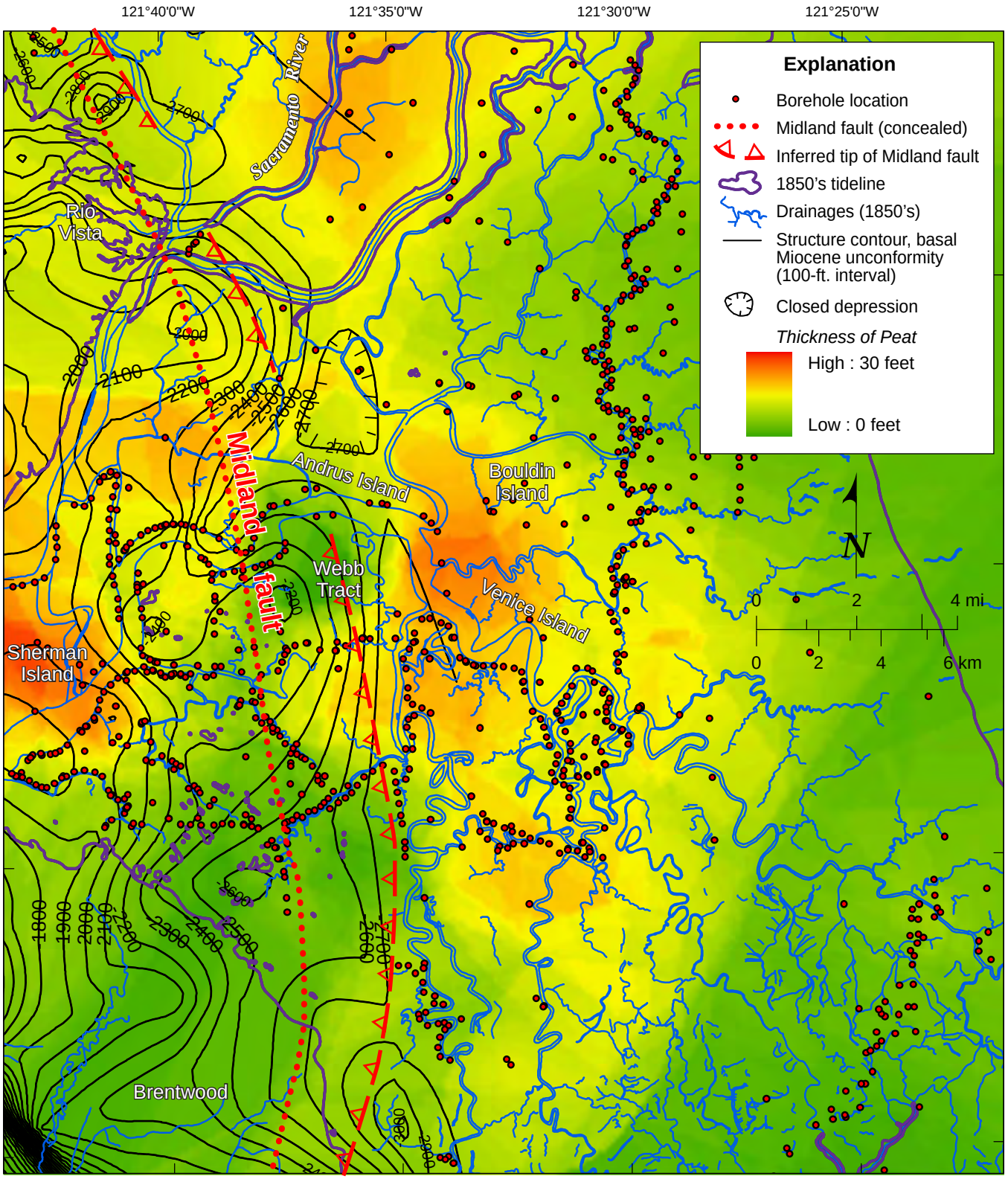

Graphics, Active Projects, 1958.000 Midland Fault, Modified 11.15.09

Thickness of Peat versus Relief on Basal Miocene Unconformity FIGURE 12

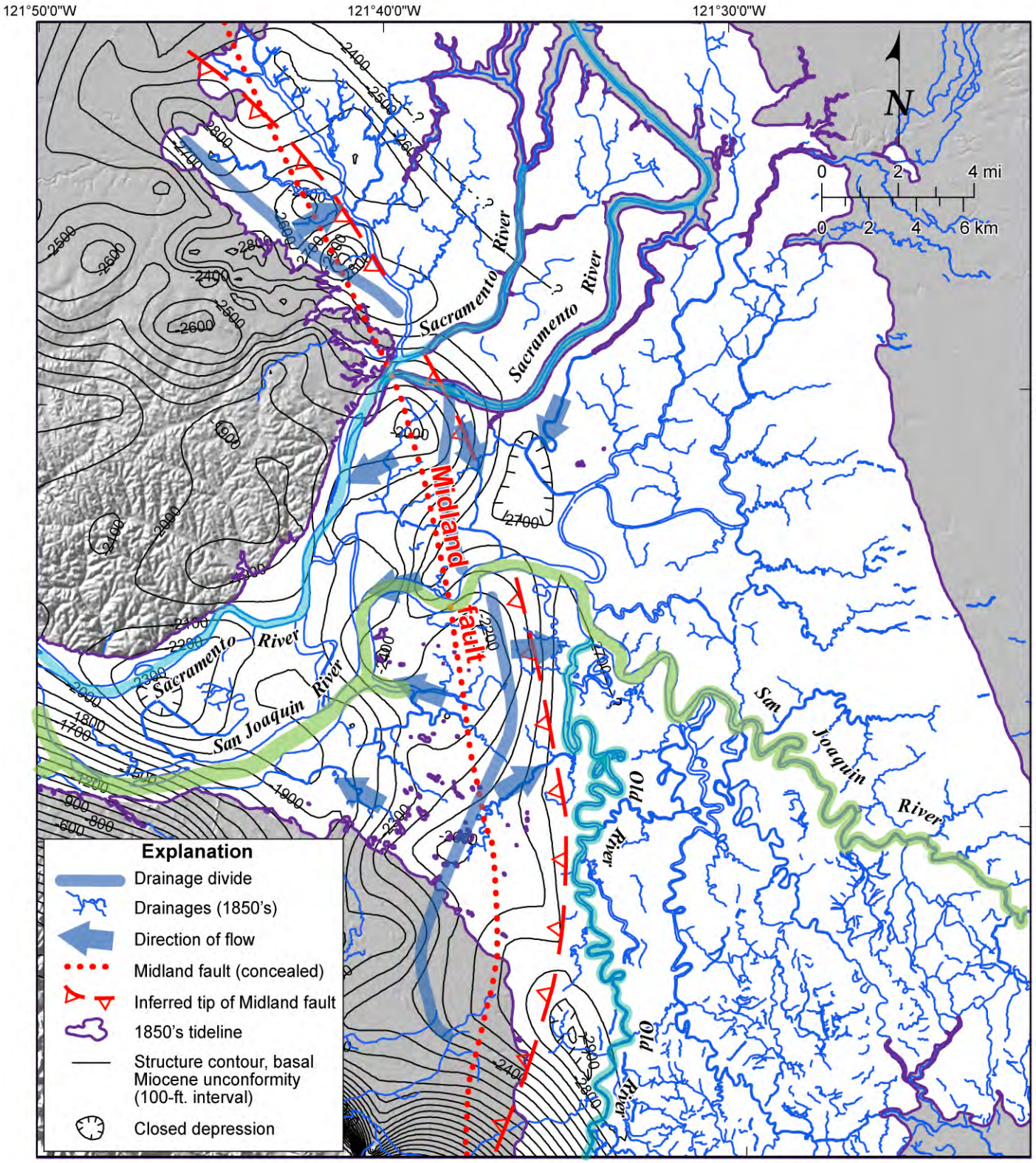

Graphics, Active Projects, 1958.000 Midland Fault, Modified 11.15.09

Historic Stream Pattern versus Underlying Structure FIGURE 13

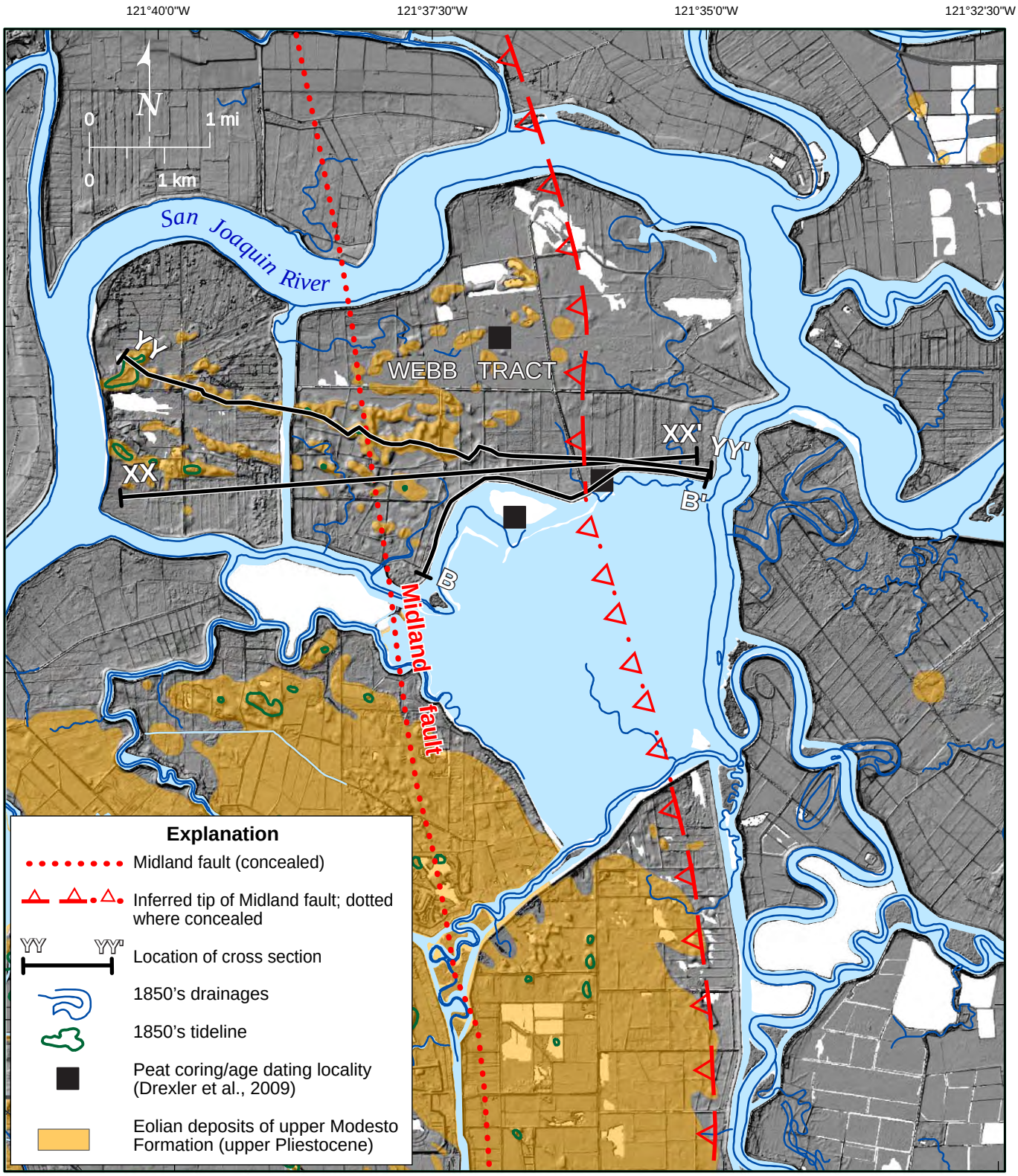

Graphics, Active Projects, 1958.000 Midland Fault, Modified 10.27.09

Distribution across Midland Fault of Eolian Deposits of Upper Modesto Formation

FIGURE 14

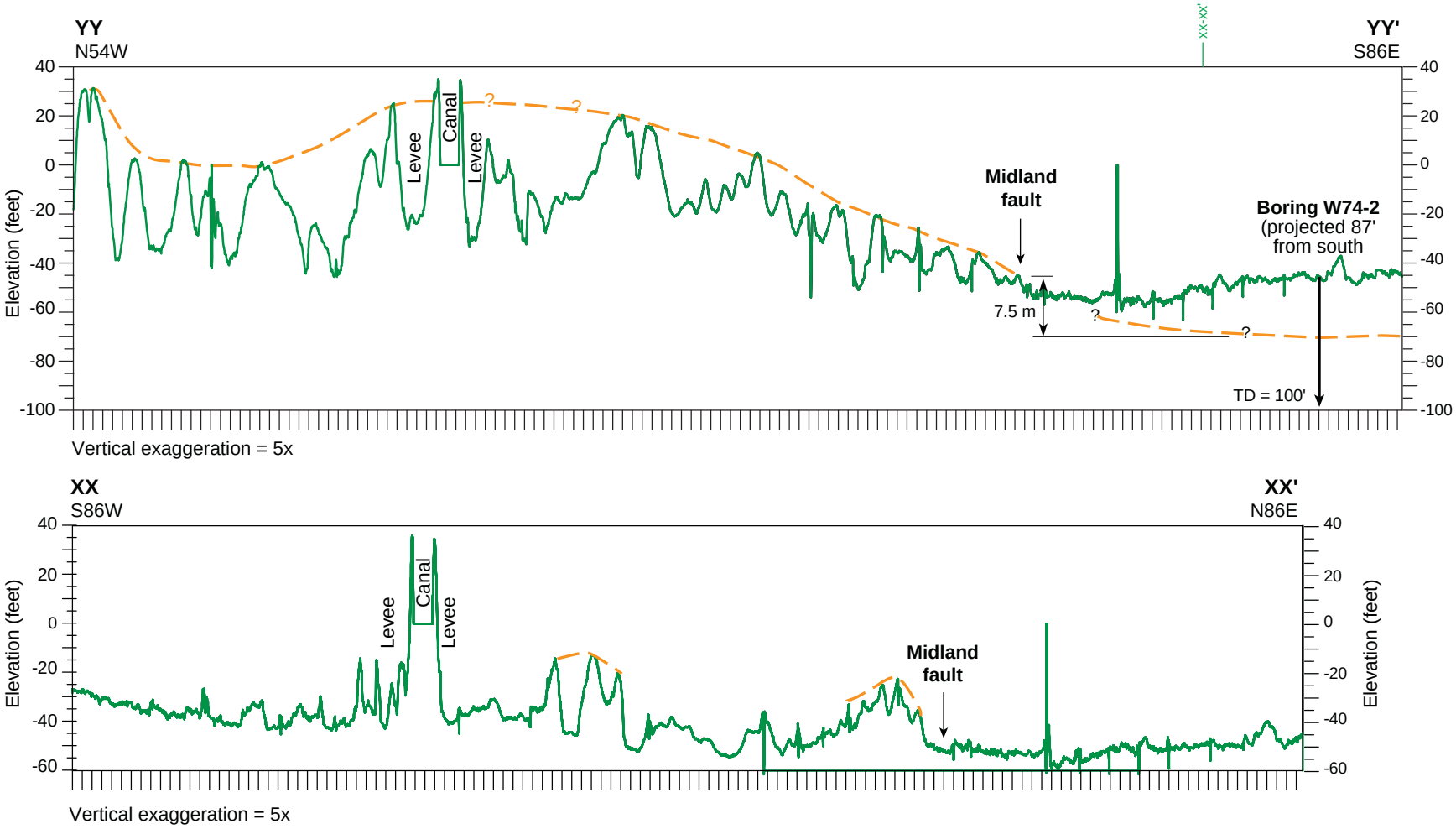

Explanation

Land surface

Approximate top of Eolian deposits of upper Modesto Formation (upper Pleistocene); dashed where approximate

Note: See Figure 14 for location of cross sections.

Topographic Profiles Showing Top of Eolian Deposits and Land Surfaces across Midland Fault

FIGURE 15

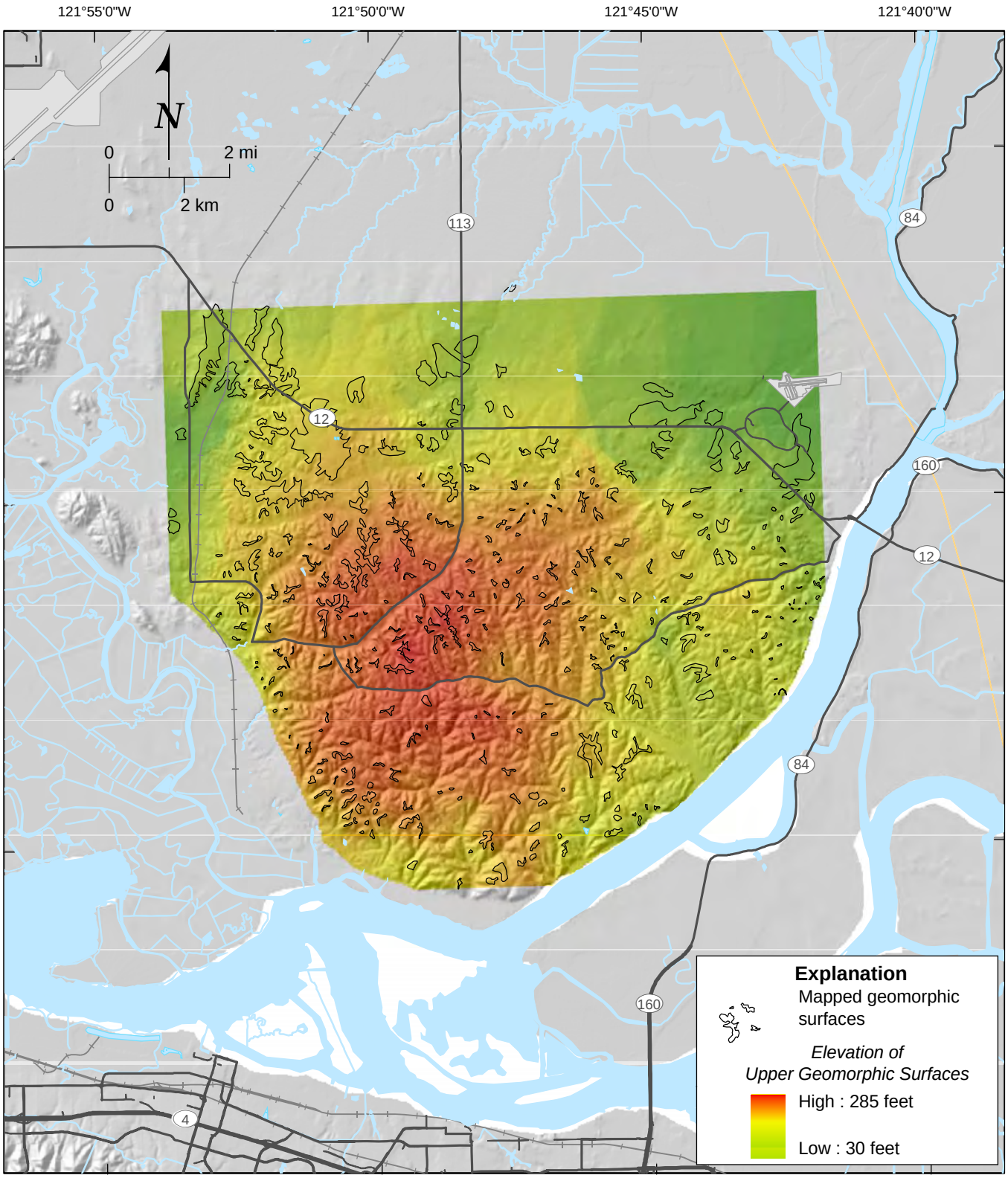

Graphics, Active Projects, 1958.000 Midland Fault, Modified 10.15.09

Envelope Map of Upper Geomorphic Surfaces, Montezuma Hills FIGURE 16

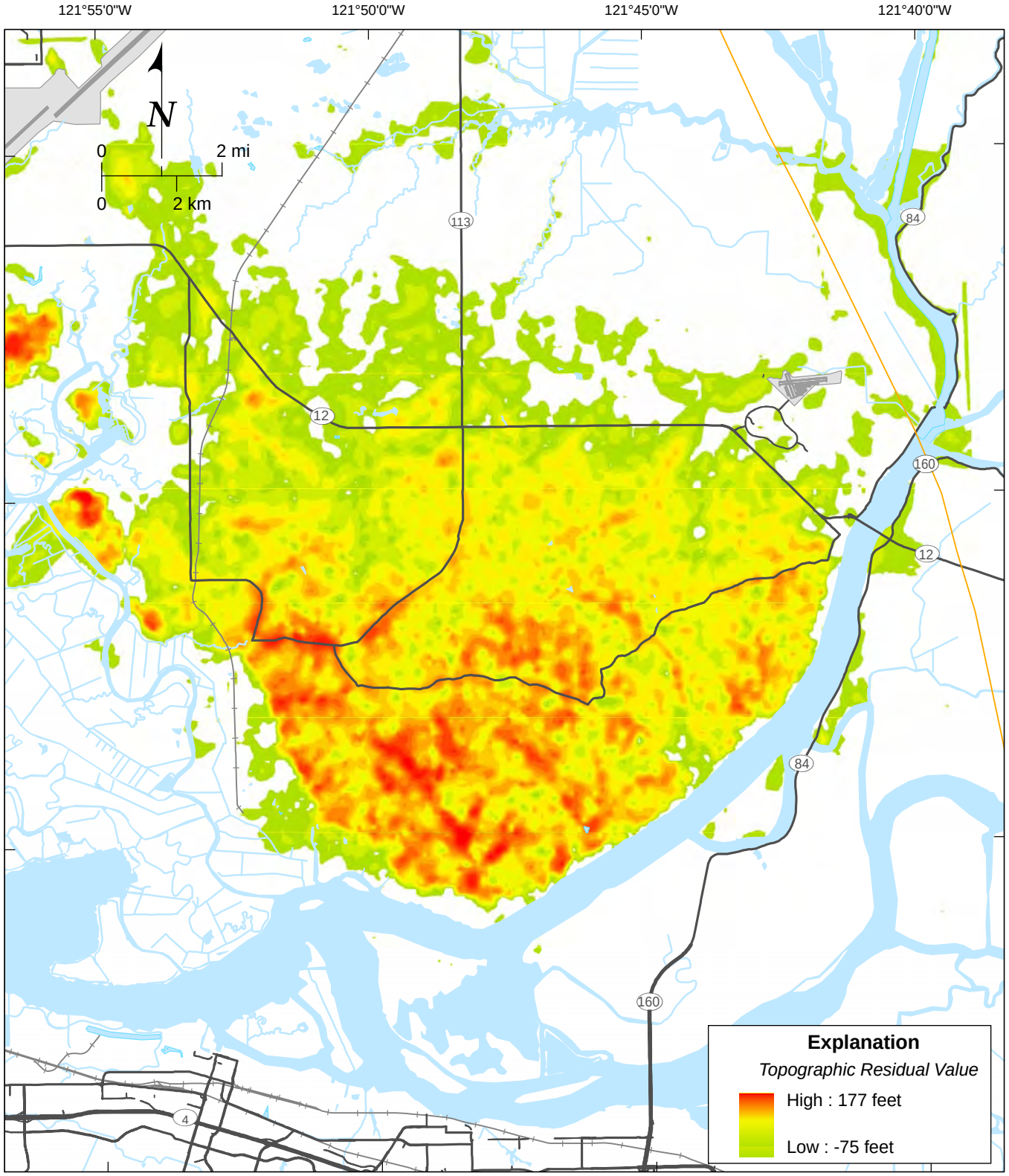

Graphics, Active Projects, 1958.000 Midland Fault, Modified 10.15.09

Residual Map of Topographic Relief, Montezuma Hills FIGURE 17